Dust in the Small Magellanic Cloud: II. Dust Models from Interstellar Polarization and Extinction Data

C. V. Rodrigues[1] and A. M. Magalhães
Inst. Astronômico e Geofísico - USP
Caixa Postal 9638
São Paulo - SP 01065-970
Brazil
e-mail: claudia@das.inpe.br, mario@argus.iagusp.usp.br

and

G. V. Coyne, S. J.
Vatican Observatory
V-00120 Vatican City State
Rome, Italy
e-mail: specola_vat@astrom.dnet.nasa.gov

ABSTRACT

We study the dust in the Small Magellanic Cloud using our polarization and extinction data (Paper I) and existing dust models. The data suggest that the monotonic SMC extinction curve is related to values of λ_{max}, the wavelength of maximum polarization, which are on the average smaller than the mean for the Galaxy. On the other hand, AZV 456, a star with an extinction similar to that for the Galaxy, shows a value of λ_{max} similar to the mean for the Galaxy.

We discuss simultaneous dust model fits to *extinction* and *polarization*. Fits to the wavelength dependent *polarization* data are possible for stars with small λ_{max}. In general, they imply dust size distributions which are narrower and have smaller mean sizes compared to typical size distributions for the Galaxy. However, stars with λ_{max} close to the Galactic norm, which also have a narrower polarization curve, cannot be fit adequately. This holds true for all of the dust models considered.

The best fits to the *extinction* curves are obtained with a power law size distribution by assuming that the cylindrical and spherical silicate grains have a *volume* distribution which is continuous from the smaller spheres to the larger cylinders. The size distribution for the cylinders is taken from the fit to the polarization. The 'typical', monotonic SMC extinction curve can be fit well with graphite and silicate grains if

---

[1]now at Inst. Nacional de Pesquisas Espaciais-INPE, Divisão de Astrofísica-DAS, Caixa Postal 515, São José dos Campos - SP 12201-970, Brazil

a small fraction of the SMC carbon is locked up in the grains. However, amorphous carbon and silicate grains also fit the data well. AZV456, which has an extinction curve similar to that for the Galaxy, has a UV bump which is too blue to be fit by spherical graphite grains.

Subject headings: ISM: dust, extinction - polarization - ultraviolet: interstellar - galaxies: Magellanic Clouds

1. INTRODUCTION

Most models currently proposed assume that the interstellar grains are formed of silicates in amorphous form and of carbon probably in the form of graphite. Mathis, Rumpl & Nordsieck (1977, hereafter MRN) have suggested homogeneous grains of silicate and graphite with a power law size distribution. Another model, which considers the grains in an evolutionary context, is advocated by Greenberg and collaborators (e.g., Hong & Greenberg 1980; Chlewicki & Greenberg 1990; hereafter the model is referred to as the CG model). They assume a trimodal grain distribution which includes: (1) grains with a silicate core and an organic refractory mantle; (2) homogeneous silicate grains; (3) graphite grains. In yet another model, that of Duley, Jones & Williams (1989, hereafter DJW), the grains are silicate nuclei covered with a hydrogenated amorphous carbon mantle. Contrary to other models, in the DJW model the 2175Å bump in the extinction curve is not produced by a graphite grain population, but is due to electronic transitions in OH^- ions within small silicate grains (Duley 1987).

The Magellanic Clouds are the nearest external galaxies. The Small Magellanic Cloud (SMC) is characterized by a small dust content which makes any study of the grains in its interstellar medium (ISM) difficult. The SMC average gas-to-dust ratio [N(H)/E(B-V)] is about 10 times that of the Galaxy (Bouchet et al. 1985), consistent with its small metallicity (e.g., Wheeler, Sneden & Truran 1989 and references therein). The most reddened stars have color excesses, E(B-V), less than 0.40^{mag} (Bouchet et al. 1985). Galactic foreground color excesses can be as large as 0.09^{mag} (Schwering 1988). The shape of the infrared (IR) extinction is similar to that of the Galaxy, with a slightly smaller value of R [=A(V)/E(B-V)] of 2.72 (Bouchet et al. 1985). In contrast, the ultraviolet (UV) extinction is very different from either that for the Galaxy or that for the Large Magellanic Cloud (LMC). It is roughly linear up to $9\mu m^{-1}$ and does not show the 2175Å bump (Prevot et al. 1984). This has often been referred to as the SMC 'typical' extinction curve.

The SMC star AZV 456 (AZV = Azzopardi & Vigneau 1982) shows an extinction and a gas-to-dust ratio (Lequeux et al. 1984) similar to the average values in the Galaxy. The interstellar lines in this direction have typical velocities for the SMC, so that the extinction is probably not foreground (Lequeux et al. 1984; Martin, Maurice & Lequeux 1989). There is an IR extended source in the SMC located at exactly the same coordinates as AZV 456 (LI-SMC 190: Schwering & Israel 1989), which also indicates that the extinction is within the SMC.

The IR emission in the SMC was studied by Sauvage, Thuan & Vigroux (1990) using IRAS data. They concluded that the weak 12μm emission is associated with a few very small grains. They attributed this to the low SMC metallicity. To explain the SMC 25μm emission they postulated the existence of a grain population of intermediate size. The only work concerning interstellar IR spectroscopy in the SMC was made by Roche, Aitken & Smith (1987). They did not detect the 9.7μm silicate band in the only HII region studied.

Bromage & Nandy (1983) and Pei (1992) studied the SMC 'typical' extinction curve using the MRN model with only spherical particles. They concluded that, by simply lowering the quantity of graphite grains relative to silicates in the Galactic models, it was possible to fit the SMC extinction without changes in the sizes used to obtain the Galactic curve. Pei (1992) and Maccioni & Perinotto (1994) have studied the extinction in the LMC and the latter noted from their fits to the extinction that no unique solution could be obtained for the grain sizes and abundance ratios.

In an effort to determine the dust properties in the SMC more accurately, Magalhães et al. (1989, 1995 [Paper I]) have for the first time obtained multicolor polarimetric data for a number of reddened SMC stars. Their data suggest that stars with the 'typical' SMC extinction, i.e., with no UV bump, have λ_{max} smaller than the average for the Galaxy. The indication is that the size distribution of the grains and not only the carbon abundance may distinguish the dust in the SMC as compared to the Galaxy. Details of that polarization data, as well as new UV extinction data, are given in Paper I.

The scope of the present work is to study the physical properties of the dust in the SMC by introducing some innovative modifications to existing dust models and applying these models to simultaneous fits of the new wavelength dependent polarization data and existing extinction data. By using *both* extinction (Lequeux et al. 1984; Prevot et al. 1984; Bouchet et al. 1985; Paper I) and polarization (Paper I) data we seek to improve our knowledge of the model parameters. In Sec. 2 we describe the models and their application to the average Galactic extinction and polarization curves. In Sec. 3 we present fits to the wavelength dependence of the SMC polarization and extinction. In Sec. 4 we discuss the main results of this work in relation to other properties of the SMC and in Sec. 5 we summarize our conclusions.

2. DESCRIPTION OF THE MODELS

Since dust multiple scattering is generally not important for the ISM in galaxies, the theoretical calculation of the interstellar extinction and polarization basically employs the average of the extinction cross sections of grains of different sizes and elongations weighted by the size distribution (e.g., Greenberg 1968). The polarization is the result of differential extinction in the two directions perpendicular to the line of sight. This can be due to anisotropies in the shape and/or in the optical properties of the grains. A model is thus defined by the size distribution and by the optical and morphological properties of the grains.

The size distribution, *n(a)*, can be represented algebraically as

$$n(a) = N f(a), \tag{1}$$

where a is the particle radius, *f(a)* describes the shape of the size distribution, and N is related to the absolute number of grains. This constant will hereafter be called the *normalization constant* and it is dependent on the elemental abundance (gas + solid phase) and on the depletion of the main grain constituents. We use the word depletion to mean the fraction of a given chemical element locked up in the grains. The abundances of interest are those of carbon (C) and silicon (Si). The calculation of the wavelength dependence of the polarization requires an assumed *f(a)*, i.e., the shape of the size distribution, but the normalization constant, N, does not need to be specified. The extinction is usually calculated by taking into account more than one grain population. Hence, we must know not only the shape of each size distribution but also the relative number of grains of each species in order to calculate their contribution to the total extinction curve.

We have considered two shapes for the grains: spheres and cylinders. The cross sections for spherical particles have been calculated using Mie theory (e.g., Bohren & Huffman 1983), while the infinite cylinder cross sections were calculated using the formulae in Lind & Greenberg (1966) for homogeneous grains and in Shah (1970) for coated grains. Those cross sections are a good approximation to spheroids and finite cylinders (e.g., Greenberg 1968; Wolff, Clayton & Meade 1993).

The elongated particles must be aligned to produce the polarization, otherwise the net effect is that of an isotropic medium. This alignment is commonly attributed to a paramagnetic relaxation mechanism arising from an imaginary part of the magnetic susceptibility. This mechanism tends to make the grains spin with their angular momentum parallel to the magnetic field, but perpendicular to the major axis of the grains (Davis & Greenstein 1951). Hildebrand (1988) has critically reviewed this and other alignment mechanisms. The degree of alignment can be described by the number distribution of grains that have a given angle between their angular momenta and the magnetic field. We have assumed a perfect alignment hypothesis, i.e., all the spinning grains having their angular momentum perfectly parallel to the magnetic field. At least with respect to the spectral dependence of the polarization this seems to approximate partial alignment situations (Chlewicki & Greenberg 1990, Fig. 1b). In any case, the angle between the magnetic field and the plane of sky, γ, must be specified.

We have considered different grain compositions. Three kinds of silicates have been used. The optical properties for the first of them, commonly called astronomical silicate, has been taken from Draine & Lee (1984), where a synthesis of laboratory and astronomical data was made. Its properties are quite similar to olivine ($[Mg, Fe]_2SiO_4$) and it shows the change in the UV slope of the extinction curve around $6.5\mu\text{m}^{-1}$ characteristic of that material. For the second of them, enstatite ($[Mg, Fe]SiO_3$), we have used the optical constants obtained by Huffman &

Stapp (1971). This material was employed by Bromage & Nandy (1983) in their fit to the typical extinction curve for the SMC and it has, in contrast to astronomical silicate, a steeper monotonic UV extinction. The third, basaltic glass (Pollack, Toon & Khare 1973; Lamy 1978), was employed by DJW in their polarization model.

The index of refraction for graphite has been taken from Draine & Lee (1984). We use the "1/3-2/3" approximation to calculate the extinction coefficients. Draine & Malhotra (1993) have recently shown that this procedure is sufficiently accurate. We have also used amorphous carbon in our models and have adopted the constants of Duley (1984). The dielectric properties of Greenberg's grain mantle are from Chlewicki & Greenberg (1990).

We now discuss in detail the influence of various parameters as one applies the different grain models to the observations. The discussion will emphasize those situations which apply to the SMC data. Throughout this work we normalize E(λ-V), the extinction curve, to E(B-V), i.e., the extinction equals 1 and zero in the B and V filters, respectively.

2.1. MRN Model

2.1.1. Extinction Parameters

In the MRN extinction model (Mathis, Rumple and Nordsiek 1977) the grains are homogeneous spherical particles of silicate and of graphite with a power law size distribution with exponent -3.5. The sizes range from 0.02μm to 0.25μm for silicate grains and from 0.005μm to 0.25μm for graphite grains. Mathis (1979, 1986), in order to model the polarization, introduced an additional population of elongated silicate grains (cylinders) with a single size distribution describing both the spherical and the elongated silicates. From a minimum grain radius, a_-^{sil}, until an intermediate radius, a_p^{sil}, the grains were assumed to be spherical (or not aligned), and from then up to a maximum radius, a_+^{sil}, they were taken as aligned cylinders. We introduce two innovations. First, in the context of the MRN models, we attempt to fit simultaneously the polarization and the extinction. To the best of our knowledge such simultaneous fits have never been attempted previously, even though, as we shall see, the combination of shapes might be expected to affect the extinction as well as the polarization. Secondly, we introduce *volume continuity* as an alternative to *size continuity*.

In a model of spherical particles, only the carbon and silicate abundances and their depletions must be specified. However, in the case of a combination of both spherical and cylindrical silicate grains the elemental fraction for each shape must also be known. In the single size distribution of Mathis (1979), when silicate cylinders and spheres of the same material have the same normalization constant, these fractions are automatically fixed by one boundary condition: the number of cylinders and spheres at the radius a_p^{sil} must be the same. Hereafter, we call this case *size continuity*. We have in addition studied the influence of a different boundary condition on the

distribution of spheres and cylinders. We employ the same shape, *f(a)*, for the size distributions of both populations, but the normalization constants of the distributions are not assumed to be the same. Specifically, we have calculated them in such a way that the volume distribution is continuous, i.e., the boundary condition is such that the total volume occupied by the spherical and by the cylindrical grains of size a_p^{sil} must be equal. This will be called *volume continuity.* The distinction between the size and volume continuities can be understood in the following manner. Let two particles be of the same radius but one being spherical and the other a prolate cylinder with an elongation equal to or greater than two. The cylindrical particle has a greater volume and, therefore, a larger number of spherical particles will be necessary in order to have the same total volume as that occupied by the cylindrical particles. Hence, the normalization constant of the silicate spheres is larger than that of the cylindrical particles. This results in a larger relative contribution by spherical particles in the case of the volume continuity as compared to size continuity. We have used an elongation of two for the cylindrical particles.

Is there a mechanism which could provide volume continuity? We suggest the possibility of the coagulation of smaller spherical grains to form cylindrical grains. If the sticking is only efficient above a given size, the initial size distribution of spherical particles would be split in two components. The spherical one would represent the smaller grains which have not coagulated. The larger cylindrical grains would be the result of grain sticking and would be related to the initial large end of the spherical grain distribution in such wise that the material volume remains the same.

In Fig. 1, we have plotted extinction curves for spherical grains only and also for a combination of spherical and cylindrical grains, using both size continuity and volume continuity. The points represent the average Galactic extinction curve of Savage & Mathis (1979). The size ranges are the ones often used in the literature and described in the first paragraph of this section. For the lower limit to the size of the silicate cylinders, a_p^{sil} , we used 0.055μm as compared to 0.08μm in Mathis (1979), because cylindrical particles ranging from 0.08μm and larger could not reproduce the Galactic polarization curve. This might be due to the fact that we used different indices of refraction than those used by Mathis (1979). The Galactic abundances have been extracted from the data of Anders & Grevesse (1989). The C depletion was assumed to be 60% (i.e., 60% of the carbon is in the form of grains) according to Draine & Lee (1984).

We see that the resultant extinction, if we include cylinders, is quite different from that obtained by using only spheres. The reason for this is that the visible extinction produced by cylindrical silicates is smaller than that produced by spheres only, so that the contribution of graphite must be increased in order to produce the same amount of extinction. The graphite bump also becomes more pronounced. Furthermore, in the classical case of size continuity the extinction in the far ultraviolet (FUV; i.e., $\lambda^{-1} > 5\mu m^{-1}$) is lowered since the extinction by silicate spheres is reduced. In the IR the amount of extinction observed is significantly smaller (i.e., smaller R) than that of the models which include cylinders. We conclude that the model using only spheres is at best an approximation.

In Fig. 2 we show a fit to the extinction using size continuity and the contribution of each of the three grain populations to the total extinction curve. The size ranges of this fit may be compared to the MRN ones from the captions to Fig. 1 and 2. One notes the saturation of the extinction by the cylindrical silicate grains in the UV (dash-dotted line), which leaves the spherical silicate grains (dashed line) as the main source of the extinction in the FUV. Graphite (dotted line) makes a significant contribution to the FUV rise and only a minor one to the IR extinction, where the cylindrical silicate grains prevail.

Fig. 2 also illustrates the flattening of the slope of the UV extinction produced by astronomical silicate, as seen, in the curve for spherical silicate at $6.5\mu\mathrm{m}^{-1}$. This feature will be important when fitting the SMC monotonic extinction curve (see sec. 3.3.1 and Fig. 13).

The bump in the Galactic extinction curve around 2200Å ($\lambda^{-1} = 4.5\mu\mathrm{m}^{-1}$) in Figs. 1 and 2 can be reproduced by the graphite and most models consider it as the carrier. This is reviewed in detail by Draine (1989). If the abundances are kept fixed, Fig. 3 shows that changes in the C depletion result in different contributions of the graphite extinction to the total curve. An increase in C depletion results in both a stronger bump and in an increase in the graphite contribution in the visible as compared to that for silicates. This in turn decreases the IR extinction, which is mostly due to silicates. The FUV curvature produced by graphite can mask the saturation by astronomical silicate around 6.5μm. However, as will be seen later (sec. 3.3.1), the SMC extinction can be fit with a small portion of C in the form of graphite and, in this case, the features of the different silicates in the UV may be more important than in the typical Galactic extinction curves.

In the following paragraphs, we discuss the influence of the size parameters on the extinction curves. We would like to stress that changes in those parameters are accompanied by changes in the normalization constant because the available material to make the grains is fixed by the abundances and depletion chosen. For instance, if we consider two size distributions with the same initial size and different maximum sizes, the one having larger maximum size has a small normalization constant since the integral of the distributions (proportional to the material consumed by the grains) must be the same.

In Figs. 4, 5, 6 and 7 we show the influence of the size distribution parameters on the extinction curve. First, Fig. 4 shows that the extinction produced by a silicate distribution extended to smaller a_-^{sil}, the lower limit of the spherical silicate size distribution, has an enhanced FUV extinction, since there are more grains contributing to the extinction towards shorter wavelengths. Fig. 5 shows the influence of a_p^{sil}, the maximum size of spherical silicates, which is also the minimum size of cylindrical silicates. The slope of the extinction after $\lambda^{-1} \approx 6.0\mu\mathrm{m}^{-1}$ increases slightly when we increase a_p^{sil} to 0.06μm. This happens because the extension of the spherical silicate population to larger sizes makes the FUV extinction (dashed line in Fig. 2) larger and more important at lower frequencies. The increase of a_p^{sil} also makes the saturation of the extinction caused by cylinders (dot-dashed line in Fig. 2) to occur at lower frequencies and at a lower level. Changes in the silicate grain sizes thus alter the level and shape of the extinction

curve. Fig. 6 shows the effect of changes in the maximum size of the cylindrical population, a_+^{sil}. Since these affect mostly the visible, the region of the normalization, the extinction changes throughout the spectrum, but more prominently in the extremes. The level of the UV extinction is greater for smaller sizes, and the shape in the IR and visible changes in such wise that larger values of R (total to selective extinction) are obtained for greater sizes.

Fig. 7 shows that changes in the parameters of the graphite population are mainly reflected in the bump in the extinction curve, but are present throughout the curve. The increase of a_-^{car}, the minimum size of graphite grains, makes the bump weaker and the FUV rise slightly steeper. The increase of a_+^{car}, the maximum size of graphite, produces weaker bumps and also reduces the level of the UV extinction. This is because with the total amount of carbon available fixed, the inclusion of larger particles makes the contribution of the smaller particles decrease. This is expressed by a small normalization constant of the size distribution. The IR extinction increases for large a_+^{car}. The variations in the bump position are relatively small when the size parameters of graphite are changed (but see sec. 3.3.2).

Kim, Martin & Hendry (1994) have recently studied the size distribution of interstellar dust from fits to extinction using the maximum entropy method. They have analyzed two extinction curves, one with R=3.1, representing the diffuse medium, and another with R=5.3, for a dense cloud region. For the R=3.1 case, their results agree qualitatively with the MRN power law, while for the dense region case the size distribution is no longer the same. The measured value of R (2.72; Bouchet et al 1985) for the SMC suggests that most of the measured extinction comes from the diffuse medium in that Galaxy, lending further support to the MRN power law which we have adopted.

Another parameter of the extinction curve is the angle between the magnetic field and the plane of sky, γ, that defines the alignment of the elongated grains. The extinction curve is practically insensitive to this parameter. The small differences that appear are such that smaller angles simulate larger grain sizes (Hong and Greenberg 1980 and references therein). Larger changes, however, are seen in the polarization (see sec. 2.1.2.).

2.1.2. Polarization Parameters

There are two approaches to the polarization within the context of the MRN model. Mathis (1979) proposed a simple replacement of a fraction of the spherical grains by cylindrical ones (as described above in the first paragraph of Sec. 2.1.1). This case will be called the MRN model. Mathis (1986, hereafter M86) proposed a modification to the above scenario. The polarizing material would consist of silicate particles containing inclusions of ferromagnetic material in order to make the alignment more efficient (Jones & Spitzer 1967). The number of these inclusions increases with grain size in such wise that larger grains have a greater probability of being aligned. This probability is given by

$$p(a) = 1 - \exp\left[-\left(\frac{a}{a'}\right)^3\right] , \tag{2}$$

where a' is the smallest size containing a superparamagnetic inclusion. In order to reproduce the K x λ_{max} relation of Wilking et al. (1980, 1982), the dependence of a' upon λ_{max} was taken as:

$$a' = 0.329\lambda_{max}^{2.17} . \tag{3}$$

Hence, a' is fixed by the observed λ_{max}. As the grains need to be aligned to produce the polarization, the effective number of grains contributing to polarization is given by the size distribution multiplied by the above probability.

The fits using M86 produce a polarization curve with the maximum towards redder wavelengths as compared to the MRN model. For instance, with a λ_{max} of 0.55μm, the value of a' is 0.09μm. Hence only the large grains are contributing to the polarization. Changes in the a_p^{sil} are important only if a' is smaller than a_p^{sil}, otherwise the smallest polarizing grain is fixed by a', which is determined by the observed wavelength dependence of the polarization.

A polarization model involves relatively few parameters: the maximum and minimum cylinder sizes, a_+^{sil} and a_p^{sil}, respectively, and the direction of the magnetic field with respect to the plane of the sky, γ. For small values of γ, the polarizing efficiency of the grains increases, and the polarization curve becomes narrower (Hong & Greenberg 1980). Moreover, λ_{max} shifts to bluer wavelengths, simulating smaller grains.

In Fig 8 we show polarization curves for various models with a fixed value of $\gamma = 10^o$. For a discussion of the CG model see Sec. 2.2 below. If we increase a_p^{sil} (from solid to dotted curve in Fig. 8), λ_{max} has a noticeable shift to redder wavelengths and the curve is modified from the UV throughout the optical. On the other hand, when a_+^{sil} is reduced (from solid to small-dashed curve in Fig. 8) only the visible and red parts of the polarization curve are altered. The UV portion remains the same since it is produced by the unchanged smaller grains.

In Fig. 9 we show the results for polarization by enstatite as compared to astronomical silicate. The curves are significantly different in both the FUV and the IR portions of the spectrum. In the optical the enstatite simulates astronomical silicates of smaller sizes as evidenced by a shift of the polarization maximum to the blue.

Kim & Martin (1994) have recently studied the size distribution of interstellar dust grains applying the maximum entropy method to the polarization. They concluded that, in order to fit the polarization, it is not necessary to have as many small particles as the size distribution inferred from extinction fits. Significatively, this is very similar to our approach for the silicate size distribution, where the small particles are spheres and the larger ones cylinders. As we do, they also suggest coagulation as a possible scenario leading to such a distribution (sec 2.1.1).

2.2. CG Model

In the CG model (e.g., Chlewicki and Greenberg 1990; Hong & Greenberg 1980), the large grains are made of a silicate nucleus covered by organic refractory material. This mantle is formed in molecular clouds by the accretion of light elements and subsequent UV photoprocessing. In addition, two populations of smaller and homogeneous grains of graphite and silicate are needed to explain the whole spectral range of the extinction data. The size distribution of the large core-mantle grains is

$$n(a) = \exp\left[-5\left(\frac{a - a_c}{a_i}\right)^3\right] \tag{4}$$

where a_c represents the core size (assumed fixed) and a_i, the decay rate of the distribution. In other words, all the large grains are assumed to have cores of the same size, while the mantles have a thickness in accordance with the above size distribution. These grains are assumed to be elongated so that they also polarize.

Hong & Greenberg (1980) have used a single size for the small bare grains. Here, however, we have adopted for the bare grains the same type of size distribution as for the core-mantle grains, but *now* a_c defines the initial size of the distribution. Chlewicki & Greenberg (1990, sec. III) have also considered this size distribution to represent the homogeneous particles.

It is necessary to determine the fraction of Si in the two silicate populations: the large core-mantle and the small bare grains. In contrast to the MRN model, we have two completely unrelated distributions and no boundary condition can be obtained. We then calculate the Si abundance in solid form required to reproduce the observed degree of polarization (the size parameters have been previously fit by using the polarization wavelength dependence). As the total Si in solid form is given by the values of the Si abundance and depletions adopted, the fractions used in the extinction modelling are simply calculated by the difference between the total abundance of solid Si and the abundance required by the observed polarization.

In general, the results obtained from varying the extinction parameters are very similar to the those in the MRN model. The consequences of the different shapes of the size distributions can be better illustrated in the polarization case when there is only one grain population. Some effects are illustrated in Fig. 8. While the maximum size of the MRN model only changes the size cutoff, a_i also modifies the shape of the size distribution. A larger a_i makes the size distribution fall off slower for larger grains, in such wise that the larger grains have greater weight.

Changing a_c in CG model is very analogous to varying a_p^{sil} in the MRN model. In addition, when astronomical silicate is replaced by enstatite, the polarization curve is only slightly changed, since the mantle is thick enough to dominate the optical behavior of the grain for typical Galactic sizes.

2.3. DJW Model

For the polarization fits (see Sec. 3.2 below), we have also considered the DJW (Duley, Jones & Williams 1989) model. In this case, the polarization is produced by core-mantle grains with a power law size distribution following the assumptions of M86. The nuclei are composed of silicates with a thin mantle of amorphous carbon. The mantle is assumed to be thin enough so that the optical properties of the whole grain are determined only by its nucleus; the composite suggested to represent this situation was basaltic glass (Lamy 1978; Pollack, Toon & Khare 1973). The practical difference between this and the M86 model is the index of refraction of the particles. Basaltic glass behaves more like enstatite than astronomical silicate, and simulates small astronomical silicate grains.

3. DUST MODELS FITS TO THE SMC DATA

We have assumed that the SMC interstellar grains can be represented by the same analytical type of size distribution as for the Galaxy but with different width and average size. This would be the case if the same processes of grain formation and evolution took place in environments of different metallicity. We have thus developed a computational code that searches for the best size parameters (within the scenario of a given model) which fit a given observed (polarization or extinction) curve. For the models based on a power law size distribution, we have used an exponent of -3.5 (MRN), with the minimum and maximum sizes considered as free parameters. For size distribution of Greenberg and collaborators (eq. 4), we have assumed the core size, a_c, and the decay parameter, a_i, as free parameters. The parameters of the models are described in Sec. 2.

Our aim is to reproduce simultaneously the polarization as well as the extinction curve. Our approach was first to compute fits to the polarimetric data in order to obtain the sizes of the anisotropic particles; these were then carried over as fixed parameters in the fits to the extinction curve.

As discussed in Sec. 2, to fit the wavelength dependence of the polarization the Si abundance does not need to be specified. For the extinction, however, the abundances of carbon and silicon must be known. We have taken these from the work of Dufton, Fitzsimmons & Howarth (1990), which provides the abundances of C, Si and other elements in the atmosphere of a main sequence B-type star in the SMC. We assume that these represent the present ISM abundance in that galaxy (Pagel 1993). The resulting carbon abundance is consistent with a SMC metal abundance of approximately 0.8-1.0 dex smaller than the Galactic one. Recently, Rolleston et al. (1993) confirmed that result. Barbuy et al. (1991), in a study of cool supergiants, also found carbon abundances consistent with the other heavy elements. Besides, the N abundance indicates no contamination of processed material in the atmosphere, which suggests that this C abundance may indeed represent the ISM. Dufour, Shields & Talbot (1982) and Dufour (1984) found a C

abundance in HII regions in the SMC to be about 1.5 dex smaller than the Galactic one. If this value really represents the ISM, it might be a consequence of C depletion in grains.

De Boer (1991) suggested a normal depletion (stellar "minus" interstellar) of the elements in the LMC relative to the Galaxy. Despite the lack of SMC data, one might assume that the depletion of the elements in the ISM of the SMC is similar to that in the Galaxy. We take the Si depletion to be equal to 1, i.e., all available silicon is in the form of grains. On the other hand, the correct fraction of carbon in solid particles is not well determined even in our Galaxy, but may range from 0.0 to 0.6 (Whittet 1984; Gondhalekar 1985a; Jenkins 1987). A dependence of this fraction on the environment density cannot be excluded (Gondhalekar 1985a,b). We have thus computed fits using a range of C depletion values.

3.1. Data

We have optical multicolor polarimetric data for six stars in the SMC: AZV 126, 211, 215, 221, 398 and 456 (Paper I). The ISM characteristics along the lines of sight to these stars are presented in Table 1 (except for AZV 126 for reasons given below). Column 1 gives the star identification number from Azzopardi & Vigneau (1982); col. 2 that from Sanduleak (1968, 1969); cols. 3 to 6 give the parameter fits to the Serkowski polarization curve (Paper I); col. 7 lists the gas to dust ratio (Bouchet et al. 1985); cols. 8, 9 and 10 give the total and cols. 11, 12 and 13 the SMC intrinsic color excess, visual extinction and polarization to extinction ratio, respectively. The intrinsic reddening values should be viewed with caution (Paper I). The Galactic foreground reddening for all objects was assumed to be 0.05^{mag}, close to the median of the values observed towards the SMC as given by Bessel (1991). Values ranging from 0.02^{mag} to 0.09^{mag} have been claimed in the literature (McNamara and Feltz 1980, Schwering 1988, Bessel 1991) for the foreground reddenning and there is an added uncertainty in the estimates of E(B-V). For AZV 126, as detailed in Paper I, a UV extinction curve could not be reliably determined in view of its relatively low reddening (comparable to the reddening of the comparison stars). Furthermore, the relatively large scatter in the polarization measurements of AZV 126 would not allow an adequate fit by the Serkowski-type law. For these reasons we omit it from further discussions.

The sample of stars can be divided into two groups according to the wavelength dependence of the polarization. One group (AZV 211, 221 and 398) is characterized in comparison to the Galaxy by small λ_{max} but with normal widths (small values of K), while the second (AZV 215 and 456) has narrow curves (large values of K) with normal values of λ_{max} (Paper I).

For the extinction fits we have considered two kinds of UV extinction curves: the one for AZV 398 (Prevot et al. 1984; Paper I) and the one for AZV 456 (Lequeux et al. 1984; Paper I). The extinction curve for AZV 398 has no bump and it has an enhanced UV extinction compared to the Galaxy, while that for AZV 456 is very similar to that for the Galaxy, but with its bump shifted to bluer wavelengths (Paper I). Following Bouchet et al. (1985) we have taken the same

IR extinction for the two stars. Since they are also among the most reddened stars in the SMC, they have well determined extinction curves.

3.2. Fits to the polarization data

In this section, we summarize the results from the fits to the observed interstellar polarization in the SMC. The fits have been made by normalizing to the largest polarization measured among the filters. In Table 2 we give the fit parameters as well as the average sizes ($\langle a \rangle$) and widths of the size distributions (cols. 4 and 5, respectively). The parameters related to the cylinder size distribution, a_- (col. 2) and a_+ (col. 3) are a_p^{sil} and a_+^{sil} in the MRN and DJW models and a_c and a_i in CG model (see sec. 2.1.1 and 2.2). The widths are the difference, a_+ - a_-. The MRN, M86 and CG models with astronomical silicate (AS) were applied to all stars as indicated in cols. 7 and 8. In addition, for AZV 398 and 456, the DJW model and two kinds of silicates (namely, astronomical silicate - AS -and enstatite - ENS) have been used. The angle between the magnetic field and the plane of the sky, γ, is taken as fixed and the fits are made using three values: 10^o, 30^o, and 60^o (col. 9). The quality of the fits is assumed to be represented by the χ^2 value (col. 10). In order to facilitate a comparison of the SMC to the Galaxy, the last two lines of the table show the standard values which fit the Galactic curve using the MRN and CG models with γ equal to 10^o. The bold-type entries in Table 2 have been plotted in the figures, indicated under the star number in col. 1. The UV extrapolation to the fits are also presented in the figures.

The star AZV 211 (Fig. 10) has a relatively broad curve, a fact mirrored by the Serkowski parameter K smaller than that for the Galaxy (see Table 1 and Paper I). While the size distribution produced by the MRN model (see col. 5, Table 2) has a width comparable to the Galactic one, the average size is smaller (col. 4, Table 2). The other models, however, follow the tendency of the other stars to have a narrow size distribution. The resulting polarization curves differ slightly in the near UV extrapolation. For smaller γ, the MRN fits produce higher polarization and smaller λ_{max} .

AZV 221 follows the SMC trend. It has small λ_{max} and K values (see Table 1 and Paper I). The resulting model parameters usually have small average sizes and narrow size distribution widths (see Table 2, cols. 4 and 5). The fits are very good as shown by the extremely small χ^2 values in col. 10 of Table 2.

The star AZV 398 has the highest polarization known in the SMC (Paper I). The models fit the data well (Fig. 11). The polarization decreases rapidly from the R to the I filter, so that it is difficult to have the models fit the two redder points simultaneously. The average sizes obtained (Table 2, col. 4) are, in general, slightly smaller than those for the Galaxy. The resulting size distribution (Table 2, col. 5) is much narrower than that for the Galaxy. For the MRN and for the CG model, we make the fits by replacing astronomical silicate with enstatite. The fits do not show substantial differences, but the MRN models with enstatite tend to have smaller values of

χ^2 (Table 2, col. 10). Actually, enstatite gives a better fit to the decrease of the polarization in the red (see Fig. 11). The value of $\langle a \rangle$ obtained with enstatite is slightly larger than that obtained using astronomical silicate, according to the discussion in Sec. 2.1.2. Similar conclusions can be drawn for the DJW model.

While the stars with small λ_{max} can be easily fit (AZV 211, 221 and 398), this is not true for the stars AZV 456 and 215. For AZV456 the fits were generally not satisfactory. This is related to the fact that it has a narrow polarization curve. Fig. 12 illustrates some of the best fits which occurred for either small values of γ or relatively narrow size distributions. The MRN fit with γ=10° (dotted line) presents a significant improvement relative to the γ=60° fit (solid line). In particular, the reddest polarization point in Fig. 12 (at 0.82μm) shows the largest deviation from the fits. Values of γ smaller than 10 were also tried but did not improve the fits.

Some fits present a bump in the UV (Fig. 12, short-dashed line). This is caused by very narrow size distributions. The polarization curve of a single grain is characterized by ripples. Such ripples are usually averaged out by a size distribution, except when the distribution is too narrow. The size distribution also makes the curve broader. The bumps are generally found in the fits with the larger values of γ. This is because small values of γ produce narrow curves, so for the large values the narrowness can only be achieved using a narrow size distribution. The M86 model behaves like the MRN one. A bump in the UV is also found in the DJW fit with γ=60°. Enstatite does not modify these results (Table 2, AZV456, col. 8 = ENS).

Nevertheless, these fits are characterized by average sizes similar to those for the Galaxy, confirming the usual relationship which is claimed between λ_{max} and the average sizes. UV and/or IR data would help us to distinguish among the above distinct possibilities.

As suggested by Wilking et al. (1980), an increase in the real part of the index of refraction can produce progressively narrower polarization curves. We have made some fits using hypothetical compounds, which have the same index of refraction throughout the spectra, in order to gain some insight as to the consequences of changing the indices of refraction. We have varied the real part of the index of refraction from 1.7 to 2.0 and the imaginary part from 0.01 to 0.05. The variation in the polarization curve is very small, less than 2% in the red and 5% in the blue. Therefore, changes in the index of refraction do not seem to be large enough to improve the results. Prolate spheroids have narrower polarization curves than infinite cylinders (Wolff et al. 1994). Whether these particles can improve the fits remains to be verified.

For some stars, often more than one range of sizes would reproduce the polarization data. They represent two minima of chi-squared. Obviously, one is only a local minimum. We thought, however, that it would be interesting to consider both of these kinds of size distributions in order to see how well they fit the extinction. Examples are the fits of AZV 221 (see Table 2, M86, γ = 60°, astronomical silicate for χ^2=0.02 and 0.65) and AZV 398 (MRN, γ = 30°, enstatite, χ^2=1.50 and 0.34). The average sizes (col. 4, Table 2) that define the size distributions are approximately the same, the main difference being in their widths (col.5, Table 2).

For all stars, we note that the average grain size decreases as γ increases (Table 2, compare cols. 4 and 9). This can be understood if one considers the geometric space defined by the rotation of a grain. Under a magnetic field with a large component in the line of sight (i.e., greater γ), the geometric space described by the rotating grain is greater (and more isotropic) than the one produced for a smaller γ. Under that condition, the grain looks larger. Average sizes obtained for different models at a given γ are basically the same. The polarizing efficiency is greater for smaller γ, due to the greater anisotropy presented by the rotating grains.

In summary, the best results of the polarization fits are obtained for stars having smaller λ_{max}. Their polarization curve can be fit for any model or choice of γ. The average sizes have a small spread, but the sizes are always smaller than the Galactic ones. The second group, formed by the stars AZV 456 and AZV 215, has very narrow curves, not easily fit by the above models. For these stars the best fits tend to require small values of γ or narrow size distributions, but a complete agreement with observations is not achieved. Changes in the index of refraction do not seem to improve the results. In general, the SMC size distribution seems to be narrower that the Galactic one. For most stars, data in other spectral regions and with more spectral resolution would help to constrain the shape of the curve and hence the properties of the polarizing grains.

3.3. Fits to the extinction curves

As mentioned earlier (Sec. 3.1) we have computed fits to the extinction for two stars: AZV 398 and AZV 456, since they should be representative of the two kinds of extinction curves found in the SMC. AZV 398 possesses a typical SMC extinction curve, while AZV 456 has an extinction similar to that for the Galaxy. These stars are also among the more reddened ones in the SMC and have relatively high polarization.

The number of free parameters depends on the specific model. In the original MRN model, there are two populations of spherical grains: graphite and silicate. In this case, four parameters are to be adjusted: the maximum and minimum size for each type of grain. In order to account for the polarization, cylindrical silicate grains must be included. Our approach was to compute first the fits to the polarization (see Sec. 3.2) and then, with the sizes of the anisotropic particles thus obtained, attempt to fit the extinction. If we assume size continuity (see Sec. 2.1.1), we have only three free parameters, namely, the maximum and minimum carbon grain sizes and the minimum silicate sizes, a_+^{car} , a_-^{car} and a_-^{sil}, respectively.

The CG model always includes the anisotropic particles. Hence, with the sizes of the cylinders fixed by the polarization, there are four free parameters related to the size distributions of spherical particles (graphite and silicates). As for the MRN model, we have considered two kinds of silicates: astronomical silicate and enstatite, since their differences may be important when fitting the UV extinction. The references used for the indices of refraction of enstatite do not present values in the IR. In these cases, we have used the value of R as an additional adjusted

point in the extinction curves.

The results are presented in Tables 3 (AZV 398) and 4 (AZV 456). We use the following acronyms for the various combinations of parameters:

- **sgr**: spherical astronomical silicate + spherical **g**raphite, MRN model;
- **egr**: spherical **e**nstatite + spherical **g**raphite, MRN model;
- **sgc**: spherical astronomical silicate + spherical graphite + **c**ylindrical astronomical silicate, MRN model;
- **egc**: spherical enstatite + spherical graphite + **c**ylindrical enstatite, MRN model;
- **sca**: spherical astronomical silicate + spherical amorphous **ca**rbon, MRN model;
- **eca**: spherical enstatite + spherical amorphous **ca**rbon, MRN model;
- **scc**: spherical astronomical silicate + spherical amorphous **c**arbon + **c**ylindrical astronomical silicate, MRN model;
- **ecc**: spherical enstatite + spherical amorphous **c**arbon + **c**ylindrical enstatite, MRN model;
- **sgg**: spherical astronomical silicate + spherical graphite + cylindrical astronomical silicate, CG model;
- **egg**: spherical enstatite + spherical graphite + cylindrical enstatite, CG model.

These acronyms are listed in the first column of Tables 3 and 4. The last line of these tables shows the size parameters which fit the Galactic extinction curve for the MRN model with only spherical particles.

3.3.1. AZV 398

Table 3 lists the parameters for the fits to AZV 398 (the notes to the table provide the description of the columns and of the symbols used) and Figs. 13 through 20 show the best fits, the entries in bold-type in Table 3. Fits with larger values of χ^2 were excluded from this table.

It is possible to find good fits for AZV398 using only spherical grains of astronomical silicate and graphite (*sgr* model), if less than 10% of the carbon is locked up in the grains (Fig. 13). This result is similar to that of Bromage & Nandy (1983) and Pei (1992), who were able to fit the SMC extinction curve using a small quantity of graphite grains. This is a direct consequence of the lack of the 2175 Å bump. The indices of refraction of enstatite (Table 3, *egr* model) allow better results than those for astronomical silicate (Table 3, *sgr* model) at the extremes of the extinction curve

in Fig. 13. The latter has an inflection around $6.5\mu m^{-1}$ after which the calculated extinction has a slope rather smaller than the one observed. The fit with astronomical silicate in the IR is also poor giving an R value (the extinction at $\lambda^{-1}= 0$ in Fig. 13) smaller than 2. The average sizes of the silicate grains ($\langle a \rangle \approx 0.001\mu$m) are smaller than those for the Galactic grains ($\langle a \rangle \approx 0.033\mu$m), with the enstatite particles being smaller than the astronomical silicate ones, although spread over a larger range of sizes. The graphite sizes are similar to those for the Galaxy. They are not critical in fitting the extinction, because of their small contribution.

Fig. 14 shows the fits obtained by including a population of anisotropic silicate particles fixed by the polarization fits (the *sgc* and *egc* models in Table 3). We have again obtained the best results in the case of small C depletions and for enstatite grains. When using the *size* continuity (see Sec. 2.1.1.) only one set of parameters fits the extinction curve. That corresponds to the fit using the narrower size distribution of the cylindrical enstatite grains with $\gamma = 30^o$ and 10% of carbon in grains. In this case, the whole extinction curve is well fit (Fig. 14, solid line). The graphite grains have a small contribution which is marginally important in the IR (Fig. 15a). The main IR and visible extinction fraction is produced by the cylindrical grains. This shows the importance of fitting extinction and polarization simultaneously. Although we have two sets of parameters which fit the polarization with enstatite grains and $\gamma = 30^o$, only one of them produces a good fit to the extinction.

For most fits, however, the *size* continuity does not give a FUV extinction as high as that observed. For instance, for astronomical silicate, we could not find a set of parameters which fit the FUV extinction even partially. By using *volume* continuity the relative contribution of spherical particles is increased making the FUV extinction higher and thus providing a better fit to the observations. The best fit has been found using the broader size distribution of enstatite grains with a value of $\gamma = 30^o$ and 25% of carbon in the grains (Fig. 14, dotted line). In this case, graphite has a contribution in the IR and visible comparable to that for cylinders, and its FUV extinction is non-negligible (Fig. 15b). Like the "spherical only" case, astronomical silicate provides a poor agreement with the observations at the extreme wavelengths. The best *sgc* results correspond to $\gamma = 10^o$ and a C depletion of 10% (Fig. 14, dashed line). Each of the two fits with enstatite shown in Fig. 14 has a smaller χ^2 value than that for astronomical silicates.

The minimum size of the silicates (a_-^{sil}; Table 3, col. 4, *sgc* and *egc* entries) is smaller than that for the Galaxy. Nevertheless, the average sizes of the graphites (Table 3, col. 12) can be either smaller (when used with astronomical silicate) or larger (with enstatite). Most parameter sets that have not been included in Table 3 due to their high chi-square values were characterized by high C depletions and large graphite grains which makes the bump more shallow. This will be further discussed early in the section on AZV456 (sec. 3.3.2).

Still in the context of the MRN model we have also examined the consequences of replacing the population of graphite grains by one of amorphous carbon particles (see also Sec. 4). The results are given in Table 3 (the entries for *sca, eca, scc* and *ecc* in Col. 1). In contrast with the

graphite case, the best fits are those with large C depletion. We first consider spherical particles only (*sca* and *eca* models). Fig. 16 illustrates that in this case both kinds of silicates produce good fits. Again the FUV portion is better fit with enstatite. Although the best fits are found for larger C depletion, the χ^2 are reasonable for any depletion. Higher C depletion makes the amorphous carbon contribution more prominent and the FUV is better fitted. This is especially true for the fits with astronomical silicate.

Each of the two enstatite (*eca*) fits in Fig. 16 corresponds to a distinct chi-square minimum. The contribution of each grain population to the total extinction curve in these fits are shown in Fig. 17. In one of them (χ^2=1.7, Fig. 17a) the size distribution of the carbon grains extends to large sizes and enstatite produces most of the extinction. The large width of the carbon grain distribution makes both the normalization constant and its contribution to the total curve small (see sec. 2.1.1). In the other fit (χ^2=2.5, Fig. 17b), the carbon particles are smaller on the average and the contribution is comparable to that of enstatite. At any rate, with any of the *sca* and *eca* fits in Table 3 (col. 6) the average sizes of the silicate particles are significantly smaller than those for the Galaxy (last line of Table 3).

In Fig 18 we show the results when cylindrical particles are included (*scc* and *ecc* models in Table 3). Enstatite produces better results than does astronomical silicate (Table 3 and Fig. 18). We note again that for astronomical silicate (Fig. 18, solid line) the FUV is only partially fit because of the saturation around $6.5\mu m^{-1}$. In any case, the better fits for size continuity are found for large values of carbon depletion. We can also see a tendency towards very small sizes of carbon when using the volume continuity (see Table 3, col. 12); these cases are characterized by a small contribution of carbon to the total curve. For size continuity, the carbon sizes are larger and the contribution by silicates is small.

For enstatite and size continuity, the better fits are found for larger carbon depletion, because in this case the carbon can fit the UV extinction (Fig. 19). On the other hand, for volume continuity the better fits are for smaller carbon depletion and the UV extinction is produced by the enstatite. With enstatite, the best results (Table 3, col. 19) were achieved with size continuity (Fig. 18).

The contribution of amorphous carbon in the IR is comparable to that of silicate (Fig. 19). The carbon grains have a size distribution (Table 3, *scc* and *ecc*, cols. 10 and 11) considerably narrower than the size distribution of graphite in the Galaxy, which is primarily determined by the a_+^{car} (Table 3, col. 12, last line). The changes in the average sizes are due mostly to the minimum carbon size (col. 10). When using amorphous carbon, the lower limit of silicate sizes, a_-, tends to be smaller than that for the Galaxy.

In Fig. 20 we show fits using the CG model (*sgg* and *egg* models). With astronomical silicates, the saturation in the region of $6.5\mu m^{-1}$ is very clear, although the IR and visible extinction are well fit (solid line, Fig. 20). This set of parameters does not have the smallest χ^2, but the IR extinction is best fit. When using enstatite, reasonable fits are found for a C depletion of 50%

(dotted line, Fig. 20), but the resulting value of R is too small.

The contribution of the cylindrical grains (not shown) is small along the whole spectrum. This may be a result of the assumptions made relative to this model. Probably, a greater contribution of the cylindrical grains would improve the fits, since in the MRN model that contribution is much more important. In Table 1 of Hong & Greenberg (1980), they present the ratio between the normalization constants of the size distributions of homogeneous silicate grains and core-mantle grains, which is approximately 200. In the plotted fit for astronomical silicate (Fig. 20, solid line), this ratio is about 20 and for enstatite (Fig. 20, dotted line) it is about 100. The smaller this ratio the greater is the contribution of cylinders compared to spheres and the better is the fit to the IR. However, the ratio in our models is always smaller than those of Hong & Greenberg (1980). The reason may be that we use a size distribution and they use a single size. Graphite is the major contributor even in the FUV. It is difficult to make a comparison with sizes in the Galaxy, since a different size distribution for the bare particles has been used.

In conclusion, the MRN model fits the extinction data for AZV 398. The models using enstatite produce slightly better results, especially in the FUV region. The silicate grains, on the average, are smaller than in the Galaxy. The MRN model with graphite and anisotropic particles of astronomical silicate (*sgc*) and size continuity does not fit the data. In this case, *volume* continuity provides good fits (the size continuity can only fit the curve with enstatite). When using graphite, the extinction can only be fit if we have a small number of carbon grains. However, amorphous carbon also allows a very good fit with a relatively large fraction of C in the form of grains. We were not able to find a set of parameters that satisfactorily reproduce the whole extinction curve of AZV 398 using the CG model with the present assumptions.

3.3.2. AZV 456

Fits to the extinction curve for AZV 456 are shown in Figs. 21 to 23 (the entries in bold-type in Table 4) and the size parameters are given in Table 4 (the notes to the table provide the description of the columns and of the symbols used). Since this star shows the 2175Å extinction bump, graphite or another compound which will reproduce the UV bump must be included.

Fig. 21 shows that models using spheres of silicates and graphite (Table 4, *sgr* and *egr* models) fit the data well. Both astronomical silicate and enstatite give similar results, but in both the FUV and the IR enstatite provides a slightly better fit (Fig. 21, dotted line). These fits were for 25% of carbon in grains, but, when using 50%, the fits are also very good. When more carbon is used, the graphite size range becomes extended, especially towards larger grain sizes (Table 4, cols. 3 and 11). This happens because large graphite grains produce shallower bumps (see Fig. 7 and associated discussion in sec. 2.1.1) and so compensate for the increased bump strength that would otherwise occur. Accordingly, the IR contribution by carbon grains also becomes greater. The average size of silicate is reduced for larger C depletions (Table 4, cols. 3 and 6). The models

with enstatite (*egr*) provide graphite sizes larger than those with astronomical silicate (*sgr*) (Table 4, col. 12). This is because enstatite shows an increase in extinction around $4.4\mu m^{-1}$, near the bump, so that the graphite contribution has to be made smaller, which implies larger graphite sizes. In both cases, however, the graphite grain sizes tend to be smaller than those for the Galaxy (see Table 4, col. 12, last line). It should be noted that the bump is not well fit (see below), since the calculated bump position is redder than that observed.

Fig. 22 shows that the MRN model with silicate divided into spheres and cylinders (Table 4, *sgc* and *egc* models) fits the extinction for AZV 456. In general, the fits using *volume* continuity are better than those using *size* continuity, and enstatite definitely gives better results. When using *size* continuity, reasonable fits can only be achieved for the small values of γ for either astronomical silicate or enstatite. The graphite contribution is important in the visible and IR (similarly to what has been shown in Fig. 2 for the Galaxy). The average sizes (Table 4, col. 12, entries *sgc* and *egc*) are greater than those for the Galaxy, but with a narrow size distribution. The a_{-}^{sil} is similar to the one for the Galaxy.

The extinction curve of AZV 456 is often referred to as a 'Galactic-type' curve. However, as discussed in Paper I, the extinction bump in AZV 456 is actually shifted to the blue (at $4.68\mu m^{-1}$) with respect to the Galactic average ($4.59\mu m^{-1}$, Fitzpatrick and Massa 1986). One of the rare, blue-positioned bumps known in the Galaxy is that of HD62542 (Cardelli and Savage 1988); only three Galactic bumps are known be centered beyond $4.65\mu m^{-1}$ (Mathis 1994). All our fits produce a bump shifted to redder wavelengths. This is because only small graphite particles show the bump at such relatively high wavenumbers (Cardelli and Savage 1988, Mathis 1994). The effect of a size distribution, which includes larger grains, is to broaden and move the overall bump to longer wavelengths. This effect can just be noticed in the upper three curves of Fig. 7 (sec. 2.1.1), where the increase in the lower size limit of the graphite particles gradually shifts the bump towards redder wavenumbers. Mathis (1994) also addresses in detail the problem of fitting the Galactic types of bump using the graphite constants of Draine and Lee (1984).

We have changed the parameters of the graphite distribution in both *sgc* and *egc* models, but found no improvement in fitting the bump. It would be interesting to perform the calculation using graphite grains of another shape. It has been argued that small prolate spheroids can shift the bump position to bluer wavelengths (Draine 1988, Mathis 1994). We must remember that spherical graphite particles are not likely, since graphite tends to form in anisotropic shapes (Czyzak, Hirth & Tabak 1982; Clayton et al. 1992).

The fits using the CG model and astronomical silicate (*sgg* model) have quite a small contribution from graphite, and so it is difficult to fit the observed extinction curve. Even for large C depletion, the curves do not reproduce the AZV 456 extinction (see the χ^2 values in Table 4, col. 19). The best fit is obtained when using enstatite (see Fig. 23 and Table 4, *egg* model). The bump is redder and the FUV extinction somewhat more enhanced than that observed. The Si fractions in core-mantle and homogeneous silicate particles (core-mantle: 0.68; homogeneous:

0.32) are completely consistent with the values (core-mantle: 0.70; homogeneous: 0.24) presented by Hong & Greenberg (1980).

In conclusion, in our attempts to fit polarization and extinction simultaneously we find, when using graphite, that enstatite and volume continuity give the best fits to both AZV 456, which has a Galactic-type extinction, and AZV 398, which has an SMC-type extinction (see Tables 3 and 4, *sgc* and *egc* models).

3.4. Abundances required to fit the observed polarization

We can also obtain the required Si/H ratio from the observed percentage of polarization (Table 2, column 6) and knowing the hydrogen column density towards the line of sight in question. This can be obtained from the gas-to-dust ratio N(H)/E(B-V) and the color excess. We have used for the gas-to-dust ratio the average value 5.2 10^{22} $cm^{-2}mag^{-1}$ determined by Bouchet et al. (1985) except for AZV 456, for which we used 6.9 10^{21} $cm^{-2}mag^{-1}$ from the same reference. The observed Si abundance in the SMC is 6.88 dex (Dufton et al. 1990).

Among the models the CG one generally requires a smaller quantity of Si, because the polarizing grains are not formed entirely of silicate, but have a mantle made of lighter elements. The required abundance decreases with γ, as the polarizing efficiency of the grains increases (section 3.2). Basically, all stars in Table 2 need a quantity of Si which is available in the SMC interstellar medium, the exception being AZV 456. This star shows a gas-to-dust ratio smaller than the normal ration for the SMC and like that of the Galaxy. Its color excess is similar to that for AZV 398, so this smaller ratio is interpreted as a smaller quantity of gas (H). It has a polarization comparable to other stars so it requires roughly the same quantity of Si, so the required ratio Si/H must be larger. The gas-to-dust ratio for AZV 456 was obtained taking into account only HI (Bouchet et al. 1985). However, if this line of sight has a considerable quantity of H_2 (Lequeux 1994), the gas-to-dust ratio will be similar to other SMC stars, therefore the required Si/H will be smaller, perhaps consistent with the SMC abundance. Schwering & Israel (1990) have detected an extended IR source coincident with AZV 456 which may possibly be associated with H_2.

3.5. A(V) and P(V)/A(V)

From the extinction and polarization fits the total extinction in the visible, A(V), and the ratio between the polarization and extinction, P(V)/A(V), may be obtained. A(V) is a measure of the total amount of dust in a given line of sight. A dust model should fit not only the spectral dependence of the extinction, but also its absolute value, A(V), which depends on the abundances and the depletion. This model A(V) can then be compared to the one which can be obtained observationally by assuming a value of R (total to selective extinction) and using the intrinsic

values of E(B-V) for the SMC from Table 1, col. 11.

As remarked in sec. 3.1 and Paper I, individual estimates of A(V) will be rather uncertain due to the range of foreground extinction estimates towards the SMC in the literature, which range from 0.02^{mag} to 0.09^{mag}, in addition to uncertainties in the E(B-V) determinations. For AZV 398, we have found a reasonable agreement of the model values, especially the *sgc* and *egc* models (Table 3, col. 13) with the observed value of 0.76 (see Table 1, col. 12). On the other hand, the A(V) values found for AZV 456 (see Table 4, col. 13) are smaller than the observed value of 0.73 (Table 1, col. 12). On the average, amorphous carbon produces more extinction than graphite does (Table 3, col. 13, *sgc* vs. *scc* and *egc* vs. *ecc* models). To a lesser extent, so does astronomical silicate as compared to enstatite.

The P(V)/A(V) ratio measures the polarizing efficiency of the grains. It does not depend on the abundance, but is a characteristic of a given model. The observed ratios are given in column 13 of Table 1. For both stars (AZV398 and AZV456) the calculated ratios are generally higher than observed, especially for the best fits, even though the models in Tables 3 and 4 cover the range of P(V)/A(V) values in Table 1. In the models, we have used perfect grain alignment. Imperfect grain alignment (Hong & Greenberg 1980) would improve the results at the cost of introducing additional parameters. The CG model provides good ratios for AZV 398; however, it does not reproduce its extinction curve.

4. DUST AND THE SMC ENVIRONMENT

The extinction and polarization data analyzed in this paper show that the SMC dust grains seem to be smaller than those in the Galaxy. Even within the SMC there seem to be variations in the average size. The line of sight which shows the bump (AZV 456) is characterized by larger grains. We have considered graphite as the bump carrier, so the curve for AZV 456 can only be fit by including a population of such particles. On the other hand, AZV 398 could be fit if either the number of graphite grains is small or if the carbon grains are amorphous. Possible implications are presented below.

We can associate the stars having small values of λ_{max} with the normal interstellar medium in the SMC (Paper I). Besides, in the line of sight to AZV 456, which seems to have larger grains, we see an IR emission associated with cold dust, which can be considered as a region with density enhancement, similar to the Galactic molecular clouds. The small gas-to-dust ratio towards this region (sec. 3.4) could be also an indication of the presence of molecular hydrogen. In the Galaxy, it is usually assumed that dense IS clouds have weaker UV extinction than the diffuse ISM. If the above logic is right, we can expect that the enhanced density will lead to the accretion of smaller grains on to the larger ones. This will increase the average size and reduce the width of the grain size distribution, as seen in the AZV456 results.

The UV bump in the Galactic extinction curve is supposed to be produced by carbon

(graphite) grains. Consequently, the lack of the bump in the SMC extinction curve is usually associated with a small quantity of carbon grains. However, there is no evidence for such a deficiency. The post main-sequence stars are supposed to be the primary source of interstellar grains. The relative number of carbon stars to normal stars in the post main-sequence stage is greater in the SMC than in the Milky Way (Lequeux 1988 and references therein). Also, the C/Si ratio seems to be comparable to the Galactic one (Dufton et al. 1990, see Sec. 3). Therefore, it is not obvious that the SMC has a smaller number of carbon grains, as implied by the fit to the AZV 398 extinction with a population of graphite particles (see Sec. 3.3.1). On the other hand, it has been argued that amorphous carbon grains are a more plausible interstellar component than graphite (Bussoletti, Colangeli & Orofino 1988 and references therein). Studies of interplanetary dust show that graphite is present only in trace amounts (Nuth 1985). Amorphous carbon has also been detected around R CrB stars (Hecht et al. 1984).

It has been suggested (Sorrel 1990) that carbon is transformed into graphite in the ISM by an annealing process caused by the interstellar radiation field (ISRF). The SMC would, in that case, be a privileged site for graphite formation because the ISRF is greater there than in the Galaxy (Lequeux 1989). But that does not seem to be the case, since the UV bump is not generally observed. Furthermore, Leene & Cox (1987) have found an anticorrelation between the ratio of 60μm to 100μm emission and the bump height, from which they conclude that the bump height gets smaller when the ISRF gets stronger. This last result is consistent with the SMC extinction data and its higher UV ISRF. If we believe the line of sight to AZV 456 is really characterized by higher densities, then the grains would be shielded from the strong ISRF, and so the carriers of the 2175Å bump (whatever they are) could survive.

A different interpretation is possible. It may be noted that in the lines of sight to AZV 398 and AZV 456, there are HII regions which have been identified as possible supernova remnants (SNR; Davies, Elliott & Meaburn 1976). If we associate the IR emission of AZV 456 with a dusty region, dust processing by shock waves may occur. Seab & Shull (1983) have proposed a possible enhancement of the UV bump in the SNR produced by a preferential destruction of large grains relative to the small ones and of silicate grains over graphite particles. The line of sight to AZV 456 is, however, characterized by the larger $\langle a \rangle$, which goes against this possibility. Hecht (1986) proposed that the bump carriers are small, hydrogen-poor carbon particles. One mechanism proposed for the loss of H is heating by supernova shock waves. These shock waves can also cause the annealing of amorphous carbon which can be converted into graphite. However, for that to be true, the mechanism must be more efficient than annealing by the ISRF. In this case, the carbon grains in the line of sight to AZV 398 are amorphous and the differences between the two extinction curves are the result of different dust processing as opposed to destruction by shock waves.

5. SUMMARY

The fits of the interstellar extinction and polarization data for the SMC allow us to draw the following conclusions:

1. We have attempted to fit a dust model to both extinction and polarization simultaneously. The inclusion of cylindrical particles that fit the polarization may significantly affect the extinction as well.

2. We have studied two different ways of fixing the ratio between the number of spherical and cylindrical silicates, namely size continuity and volume continuity. Fits using volume continuity, which implies a larger number of spheres, resulted in better fits. Coagulation might explain such behavior.

3. Grain models can better fit those SMC polarization curves which have small λ_{max} and normal width than they can those curves which have normal λ_{max} and narrow width. For the latter, small values of γ, the angle between the magnetic field and the plane of the sky, and narrow size distributions tend to provide the best fits, even though a completely satisfactory agreement with observations is not achieved. Extension of the spectral range covered by the polarization data in the SMC is very desirable.

4. The 'typical' SMC extinction curve can be fit using the MRN silicate- graphite model and small carbon depletion. If carbon is in an amorphous form, good results can still be obtained without the assumption of a small amount of carbon in grains.

5. The extinction curve of AZV 456, which is similar to that for the Galaxy, can be fit by the MRN model, but the bump position is not well reproduced. The calculated bump is at redder wavelengths than the observed one. Quantitative analyses using anisotropic graphite particles must still be made.

6. The core-mantle silicate model does not fit the 'typical' SMC extinction curves and only roughly reproduces the Galactic-type curve for AZV 456.

7. In general, the SMC polarization and extinction data are best fit using distributions which are narrower and shifted to smaller wavelengths relative to the Galaxy.

8. A possible scenario for the SMC is that, in the more diffuse regions, the carbon grains are in amorphous form, despite the more intense radiation field.

This work has been supported by NASA Grant NAG 5 1463. It has been also partially supported by FAPESP (CVR: 89/3091-6; AMM: 89/1670-9, 92/3345-0 and 94/0033-3) and CNPq (AMM: 301558/79-5). The programs have been run at the Department of Astronomy,

Instituto Astronômico e Geofísico, Universidade de São Paulo. AMM and CVR would like to acknowledge the hospitality provided by Dr. A. Code, Space Astronomy Laboratory and Astronomy Department, University of Wisconsin, where this research was partly done. We thank F. Vrba, J. A. Marcondes-Machado and W. J. Maciel for their critical reading of the manuscript.

REFERENCES

Anders, E. & Grevesse, N. 1989, Geochimica et Cosmochimica Acta 53, 197

Azzopardi, M. & Vigneau, J. 1982, A&AS50, 291

Barbuy, B., Spite, M., Spite, F. & Milone, A. 1991, A&A247, 15

Bessel, M.S. 1991, A&A242, L17.

Bohren, C. E. & Huffman, D. R. 1983, Absorption and Scattering by Small Particles (New York: John Wiley & Sons)

Bouchet, P., Lequeux, J., Maurice, E., Prevot, J. & Prevot-Burnichon, M. L. 1985, A&A149, 330

Bromage, G. E. & Nandy, K. 1983, MNRAS204, 29p

Bussoletti, E., Colangeli, L. & Orofino 1988, in Experiments Cosmic Dust Analogues, ed. E. Bussoletti, C. Fusco & G. Longo (Netherlands: Kluwer Ac. Publ.), 63

Cardelli, J.A. & Savage, B. D. 1988, ApJ325, 864

Chlewicki, G. & Greenberg, J. M. 1990, ApJ365, 230 (CG)

Clayton, G. C., Anderson, C. M., Magalhães, A. M., Code, A. D., Nordsieck, K. H., Meade, M. R., Wolff, M. J., Babler, B., Bjorkman, K. S., Schulte-Ladbeck, R. E., Taylor, M. & Whitney, B. A. 1992, ApJ385, L53

Czyzak, S. J., Hirth, J. P. & Tabak, R. G. 1982, Vistas in Astr. 25, 337

Davies, R. D., Elliott, K. H. & Meaburn, J. 1976, MmRAS. 81, 89

Davis, Jr., L. & Greenstein, J. L. 1951, ApJ114, 206

de Boer, K. S. 1991, in IAU Symp. 148, The Magellanic Clouds, ed. R. Haynes & D. Milne (Netherlands: Kluwer Ac. Publ.), 401

Draine, B. T. 1988, ApJ333, 848

Draine, B. T. 1989, in IAU Symp. 135, Interstellar Dust, ed. L. J. Allamandola & A. G. G. M. Tielens (Netherlands: Kluwer Ac. Publ.), 313

Draine, B. T. & Lee, H. M. 1984, ApJ285, 89

Draine, B. T. & Malhotra, S. 1993, ApJ414, 632

Dufour, R. J. 1984, in IAU Symp. 108, Structure and Evolution of the Magellanic Clouds, ed. S. van den Bergh & K. S. de Boer (Netherlands: Dordrech-Reidel), 353

Dufour, R. J., Shields, G. A. & Talbot, R. J. 1982, ApJ252, 461

Dufton, P. L., Fitzsimmons, A. & Howarth, I. D. 1990, ApJ362, L59

Duley, W. W. 1984, ApJ287, 694

Duley, W. W. 1987, MNRAS229, 203

Duley, W. W., Jones, A. P. & Williams, D. A. 1989, MNRAS236, 709 (DJW)

Fitzpatrick,, E.L. & Massa, D., 1986, ApJ307, 286

Gondhalekar, P. M. 1985a, ApJ293, 230

Gondhalekar, P. M. 1985b, MNRAS216, 57p

Greenberg, J. M. 1968, in Stars and Stellar Systems, Vol. 7, Nebulae and Interstellar Matter, ed. B. M. Middlehurst & L. H. Aller (Chicago: Univ. Chicago Press), 221

Hecht, J. 1986, ApJ305, 817

Hecht, J. Holm, A. V., Donn, B. & Wu, C. C. 1984, ApJ280, 228

Hildebrand, R. H. 1988, QJRAS. 29, 327

Hong, S. S. & Greenberg, J. M. 1980, A&A88, 194

Huffman, D. R. & Stapp, J. L. 1971, Nature Phys. Sci. 229, 45

Jenkins, E. B.1987, in Interstellar Processes, ed. D. J. Hollenbach & H. A. Thronson Jr. (Netherlands: Dordrech-Reidel), 533

Jones, R. V. & Spitzer Jr., L. 1967, ApJ147, 943

Kim, S.-H. & Martin, P. G. 1994, ApJ431, 783

Kim, S.-H., Martin, P. G & Hendry, P. D. 1994, ApJ422, 164

Lamy, P. L. 1978 Icarus 34, 68

Leene, A. & Cox, P. 1987, ApJ174, L1

Lequeux, J. 1988, in Dust in the Universe, ed. E. M. Bailey & D. A. Williams (Cambridge: Cambridge Univ. Press), 449

Lequeux, J. 1989, in Recent Developments of Magellanic Cloud Research, ed. K. S. de Boer, F. Spite & G. Stasinska (Paris: Obs. Paris), 119

Lequeux, J. 1994, A&A, 287, 368

Lequeux, J., Maurice, E., Prevot, L., Prevot-Burnichon, M. L. & Rocca-Volmerange B. 1984, A&A113, L5

Lind, A. C. & Greenberg, J. M. 1966, J. Appl. Phys. 37, 3195

Maccioni, A. & Perinotto, M. 1994, A&A284, 241

Magalhães, A. M., Rodrigues, C. V., Piirola, V. & Coyne, G. V. 1989, in IAU Symp. 135: Interstellar Dust, NASA-CP 3036, ed. L. J. Allamandola & A. G. G. M. Tielens, p. 347

Magalhães, A. M., Rodrigues, C. V., Coyne, G. V. & Piirola, V. 1995, ApJ, submitted [Paper I].

Martin, N., Maurice, E. & Lequeux, J. 1989, A&A215, 219

Mathis, J. 1979, ApJ232, 747

Mathis, J. 1986, ApJ308, 281 (M86)

Mathis, J. S. 1994, ApJ422, 176

Mathis, J., Rumpl, W. & Nordsieck, K. H. 1977, ApJ217, 425 (MRN)

McNamara, D. H. and Feltz, K. A. PASP92, 587

Nuth, J. A. 1985, Nature 318, 166

Pagel, B.E.J. 1993, in News Aspects of Magellanic Cloud Research, eds. B. Baschek, G. Klare and J. Lequeux (Berlin: Springer-Verlag), 330

Pei, Y. C. 1992, ApJ395, 130

Pollack, J. B., Toon, O. B. & Khare, B. N. 1973, Icarus 19, 372

Prevot, M. L., Lequeux, J., Maurice, E., Prevot, L. & Rocca-Volmerange, B. 1984, A&A132, 389

Roche, P. F., Aitken, D. K. & Smith, C. H. 1987, MNRAS228, 269

Rolleston, W. R. J., Dufton, P. L., Fitzsimmons, A., Howarth, I. D. & Irwin, M. J 1993, A&A277, 10

Sanduleak, N. 1968, AJ73, 246

Sanduleak, N. 1969, AJ74, 877

Sauvage, M., Thuan, T. X. & Vigroux, L. 1990, A&A237, 296

Savage, B. D. & Mathis, J. 1979, ARA&A17, 73

Schwering, P. B. W. 1988, Ph.D. Thesis, University of Leiden

Schwering, P. B. W. & Israel, F. P. 1989, A&AS79, 79

Seab, C. G. & Shull, J. M. 1983, ApJ275, 652

Shah, G. A.1970, MNRAS148, 93

Sorrell, W. H. 1990, MNRAS243, 570

Wheeler, J. C., Sneden, C. & Truran Jr., J. W. 1989, ARA&A27, 279

Whittet, D. 1984, MNRAS210, 479

Wilking, B. A., Lebofsky, M. J., Martin, P. G., Rieke, G. H. & Kemp, J. C. 1980, ApJ235, 905

Wilking, B. A., Lebofsky, M. J. & Rieke 1982, AJ87, 905

Wolff, M. J., Clayton, G.C. & Meade, M.R. 1993, ApJ403, 722

Wolff, M.J., Clayton, G.C., Martin, P.G. & Schulte-Ladbeck, R.E. 1994, ApJ423, 412

TABLE 1

CHARACTERISTICS OF THE ISM IN THE DIRECTION OF OBSERVED STARS IN THE SMC

Identification							Total			Intrinsic		
AZV	SK	λ_{max}[a] (μm)	$\sigma_{\lambda_{max}}$[a] (μm)	K[a]	σ_K[a]	$\frac{N(H)}{E(B-V)}$[b] ($cm^{-2}mag^{-1}$)	E(B-V) (mag)	A(V)[d] (mag)	$\frac{P(V)}{A(V)}$ ($\%mag^{-1}$)	E(B-V) (mag)	A(V)[d] (mag)	$\frac{P(V)}{A(V)}$ ($\%mag^{-1}$)
(1)	(2)	(3)	(4)	(5)	(6)	(7)	(8)	(9)	(10)	(11)	(12)	(13)
211	74	0.42	0.06	0.70	0.10	...	0.14[c]	0.38	3.08	0.09	0.25	3.49
215	76	0.48	0.12	0.81	0.20	$9.2\ 10^{22}$	0.12[b]	0.33	2.75	0.07	0.19	3.90
221	77	0.34	0.14	0.57	0.23	...	0.14[c]	0.38	2.66	0.09	0.25	3.35
398	...	0.40	0.05	0.68	0.08	$4.1\ 10^{22}$	0.37[b]	1.01	2.02	0.32	0.87	2.01
456	143	0.59	0.03	0.98	0.06	$6.9\ 10^{21}$	0.36[b]	0.98	1.37	0.31	0.84	1.42

[a]Magalhães et al. 1995 (Paper I)

[b]Bouchet et al. 1985

[c]Estimate

[d]Calculated with R_{SMC}= 2.72 (Bouchet et al. 1985)

NOTE.—Columns: (1) Star number by Azzopardi & Vigneau (1982); (2) Star number by Sanduleak (1968,1969); (3) and (4) Wavelength of maximum polarization and error; (5) and (6) Serkowski parameter and error; (7) Gas to dust ratio; (8) - (10) and (11) - (13) Color excess, extinction and polarization to extinction ratio.

Table 2. Parameters obtained from fits to the SMC polarimetric data

Object/ Figure (1)	a_- (μm) (2)	a_+ (μm) (3)	$\langle a \rangle$ (μm) (4)	Width (μm) (5)	$\delta(Si)^a$ (dex) (6)	Model (7)	Mat. (8)	γ (^{o}) (9)	χ^2 (10)
AZV211	0.026	0.246	0.042	0.220	6.95	MRN	AS	60	0.26
Fig. 10	**0.032**	**0.235**	**0.051**	**0.203**	**6.40**	**MRN**	**AS**	**30**	**0.21**
	0.035	**0.251**	**0.056**	**0.216**	**6.27**	**MRN**	**AS**	**10**	**0.32**
	0.014	0.106	0.041	0.092	7.09	M86	AS	60	1.42
	0.021	0.138	0.049	0.117	6.47	M86	AS	30	0.23
	0.030	0.185	0.060	0.155	6.29	M86	AS	10	0.37
	0.020	0.064	0.039	0.044	5.69	CG	AS	60	0.89
	0.026	0.081	0.049	0.055	5.24	CG	AS	30	0.58
	0.030	**0.106**	**0.062**	**0.075**	**5.07**	**CG**	**AS**	**10**	**0.31**
AZV215	0.038	0.136	0.056	0.097	6.52	MRN	AS	60	1.79
	0.048	0.067	0.056	0.019	6.33	MRN	AS	60	0.39
	0.048	0.152	0.070	0.104	6.01	MRN	AS	30	2.09
	0.054	0.187	0.080	0.133	5.90	MRN	AS	10	2.32
	0.026	0.137	0.065	0.111	7.00	M86	AS	60	3.18
	0.027	0.150	0.068	0.123	6.40	M86	AS	30	3.58
	0.047	0.065	0.056	0.018	7.03	M86	AS	60	0.40
	0.070	0.071	0.070	0.002	6.31	M86	AS	30	0.50
	0.049	0.022	0.056	-0.027	6.16	CG	AS	60	0.41
	0.067	0.010	0.070	-0.056	5.85	CG	AS	30	0.55
	0.102	0.012	0.105	-0.090	5.79	CG	AS	10	0.68
AZV221	0.028	0.141	0.043	0.113	6.50	MRN	AS	60	0.15
	0.035	0.152	0.053	0.117	5.99	MRN	AS	30	0.14
	0.044	0.159	0.065	0.116	5.85	MRN	AS	10	0.13
	0.025	0.080	0.042	0.055	6.53	M86	AS	60	0.02
	0.010	0.130	0.033	0.120	6.69	M86	AS	60	0.65
	0.026	0.149	0.048	0.123	6.05	M86	AS	30	0.16
	0.037	0.172	0.059	0.135	5.89	M86	AS	10	0.14
	0.021	0.054	0.037	0.033	5.53	CG	AS	60	0.09
	0.025	0.070	0.046	0.045	4.99	CG	AS	30	0.08
	0.033	0.089	0.059	0.056	4.93	CG	AS	10	0.16
AZV398	0.031	0.149	0.048	0.119	6.41	MRN	AS	60	1.62

Table 2—Continued

Object/ Figure (1)	a_- (μm) (2)	a_+ (μm) (3)	$\langle a \rangle$ (μm) (4)	Width (μm) (5)	$\delta(Si)^a$ (dex) (6)	Model (7)	Mat. (8)	γ (°) (9)	χ^2 (10)
Fig. 11	**0.037**	**0.172**	**0.057**	**0.135**	**5.91**	**MRN**	**AS**	**30**	**1.57**
	0.060	0.136	0.081	0.076	5.72	MRN	AS	10	1.11
	0.043	0.088	0.056	0.046	6.54	MRN	ENS	60	0.34
	0.045	0.186	0.069	0.141	6.16	MRN	ENS	30	1.50
	0.061	**0.099**	**0.075**	**0.038**	**6.05**	**MRN**	**ENS**	**30**	**0.34**
	0.076	0.141	0.098	0.065	5.96	MRN	ENS	10	1.26
	0.031	0.082	0.047	0.051	6.38	M86	AS	60	0.48
	0.009	0.140	0.032	0.131	6.60	M86	AS	60	2.36
	0.031	0.168	0.053	0.137	5.96	M86	AS	30	1.63
	0.034	0.202	0.058	0.168	5.83	M86	AS	10	1.69
	0.024	0.056	0.041	0.031	5.51	CG	AS	60	1.09
	0.039	**0.061**	**0.057**	**0.022**	**5.24**	**CG**	**AS**	**30**	**1.07**
	0.051	0.079	0.075	0.028	5.16	CG	AS	10	1.59
	0.025	0.058	0.042	0.034	5.68	CG	ENS	60	0.97
	0.051	0.051	0.066	-0.000	5.64	CG	ENS	30	1.02
	0.069	0.069	0.089	0.001	5.55	CG	ENS	10	1.72
	0.026	0.172	0.042	0.146	6.69	DJW	BAS	60	1.42
	0.044	0.196	0.067	0.152	6.12	DJW	BAS	30	1.34
	0.079	0.157	0.103	0.079	5.92	DJW	BAS	10	0.86
AZV456	**0.045**	**0.145**	**0.066**	**0.108**	**7.25**	**MRN**	**AS**	**60**	**6.43**
Fig. 12	0.056	0.160	0.080	0.104	6.74	MRN	AS	30	7.24
	0.099	**0.131**	**0.112**	**0.032**	**6.56**	**MRN**	**AS**	**10**	**1.93**
	0.109	0.166	0.131	0.057	7.72	MRN	ENS	60	2.21
	0.047	0.202	0.072	0.155	7.57	MRN	ENS	60	10.07
	0.131	0.173	0.149	0.042	7.15	MRN	ENS	30	12.94
	0.062	0.192	0.090	0.130	7.02	MRN	ENS	30	10.29
	0.084	0.200	0.116	0.116	6.87	MRN	ENS	10	4.67
	0.112	0.145	0.126	0.032	6.81	MRN	ENS	10	1.72
	0.038	0.144	0.075	0.107	7.64	M86	AS	60	11.44
	0.047	0.157	0.084	0.111	7.01	M86	AS	30	10.72
	0.055	0.184	0.094	0.129	6.78	M86	AS	10	6.52
	0.049	**0.034**	**0.059**	**-0.015**	**6.82**	**CG**	**AS**	**60**	**0.86**
	0.068	0.023	0.075	-0.046	6.48	CG	AS	30	3.29

Table 2—Continued

Object/ Figure (1)	a_- (μm) (2)	a_+ (μm) (3)	$\langle a \rangle$ (μm) (4)	Width (μm) (5)	$\delta(Si)$[a] (dex) (6)	Model (7)	Mat. (8)	γ (^{o}) (9)	χ^2 (10)
	0.099	**0.039**	**0.111**	**-0.061**	**6.41**	**CG**	**AS**	**10**	**2.01**
	0.054	0.031	0.063	-0.024	7.10	CG	ENS	60	1.03
	0.074	0.020	0.080	-0.054	6.73	CG	ENS	30	8.45
	0.118	0.028	0.126	-0.090	6.71	CG	ENS	10	1.92
	0.052	0.085	0.064	0.033	7.77	DJW	BAS	60	2.08
	0.061	0.185	0.087	0.124	7.10	DJW	BAS	30	11.56
	0.116	0.158	0.134	0.042	6.78	DJW	BAS	10	3.24
Galaxy	0.055	0.25	0.084	0.195	...	MRN	AS	10	-
	0.038	0.14	0.079	0.102	...	CG	AS	10	-

[a]The observed value of the SMC Si abundance is 6.88 (Dufton et al. 1990).

Note. — Columns: (1) The object name in the Azzopardi & Vigneau (1982) catalogue; (2) The minimum size of cylindrical grain. In the MRN model, it is called a^p_{sil}. In Greenberg's model, a_c; (3) Related to the maximum size of cylindrical grain. In the MRN model, it is a^+_{sil}. In Greenberg's model, a_i; (4) Average size; (5) Width of the size distribution which corresponds to the difference between the two size parameters (in both models); (6) Silicon abundance needed to reproduce the degree of polarization; (7) Models: MRN (Mathis, Rumpl & Nordsieck 1977), M86 (Mathis 1986) or CG (Chlewicki & Greenberg 1990); (8) Material used in the calculations: AS (astronomical silicate), ENS (Enstatite), BAS (Basaltic glass). See Sec. 2 for references; (9) Angle between the magnetic field and the plane of sky and (10) The value of χ^2 is not divided by N.

Note. — The fits in bold-face type are plotted in the figures whose numbers are given in column 1.

TABLE 3

SIZE PARAMETERS OBTAINED FITTING AZV 398 EXTINCTION CURVE

Type/ Fig. (1)	Cont. (2)	Depl. (3)	Spherical silicate a_-/a_c (μm) (4)	Spherical silicate a_+/a_i (μm) (5)	Spherical silicate $\langle a \rangle$ (μm) (6)	Cylindrical silicate a_-/a_c (μm) (7)	Cylindrical silicate a_+/a_i (μm) (8)	Cylindrical silicate $\langle a \rangle$ (μm) (9)	Carbon a_-/a_c (μm) (10)	Carbon a_+/a_i (μm) (11)	Carbon $\langle a \rangle$ (μm) (12)	A(V) Total (mag) (13)	A(V) Carbon (mag) (14)	A(V) Sp.sil. (mag) (15)	A(V) Cyl.sil. (mag) (16)	$\frac{P(V)}{A(V)}$ ($\frac{\%}{mag}$) (17)	γ (°) (18)	χ^2 (19)
sgr	...	0.10	0.0005	0.171	0.0008	...	...	...	0.0049	0.205	0.0081	-	-	-	-	-	-	7.9
13	...	0.05	0.0010	0.172	0.0016	...	...	...	0.0049	0.202	0.0081	-	-	-	-	-	-	6.7
egr	...	0.10	0.0001	0.281	0.0002	...	...	...	0.0059	0.440	0.0098	-	-	-	-	-	-	1.9
13	...	0.05	0.0006	0.290	0.0010	...	...	...	0.0051	0.203	0.0085	-	-	-	-	-	-	2.1
sgc	v	0.10	0.0053	0.031	0.0083	0.0306	0.149	0.0471	0.0001	0.066	0.0002	0.660	0.084	0.547	0.029	3.9	60	9.9
14	v	0.10	0.0060	0.060	0.0097	0.060	0.136	0.0812	0.0046	0.074	0.0076	0.822	0.111	0.666	0.045	15.9	10	5.0
	v	0.25	0.0113	0.037	0.0165	0.0370	0.172	0.0568	0.0001	0.099	0.0002	0.917	0.290	0.594	0.033	8.9	30	8.6
egc/14,15	s	0.10	0.0008	0.061	0.0013	0.0608	0.099	0.0746	0.0706	0.156	0.0949	0.559	0.224	0.327	0.008	10.6	30	3.3
	v	0.10	0.0009	0.045	0.0015	0.0455	0.186	0.0686	0.0156	0.057	0.0231	0.482	0.102	0.377	0.003	9.4	30	3.4
	v	0.10	0.0051	0.076	0.0084	0.0765	0.141	0.0978	0.0155	0.153	0.0251	0.605	0.172	0.414	0.019	12.4	10	3.8
14,15	v	0.25	0.0100	0.045	0.0153	0.0455	0.186	0.0686	0.0152	0.156	0.0247	0.810	0.428	0.377	0.005	5.6	30	3.3
sca	...	0.25	0.0015	0.266	0.0025	...	...	...	0.0016	0.043	0.0026	-	-	-	-	-	-	1.9
	...	0.50	0.0046	0.244	0.0076	...	...	...	0.0023	0.032	0.0037	-	-	-	-	-	-	1.3
	...	0.75	0.0074	0.233	0.0123	...	...	...	0.0061	0.022	0.0091	-	-	-	-	-	-	1.1
16	..	0.90	0.0078	0.228	0.0129	...	...	...	0.0061	0.020	0.0089	-	-	-	-	-	-	1.1
eca	...	0.25	0.0073	0.283	0.0120	...	...	...	0.0057	0.026	0.0088	-	-	-	-	-	-	2.2
	...	0.50	0.0074	0.273	0.0122	...	...	...	0.0049	0.020	0.0073	-	-	-	-	-	-	2.2
	...	0.50	0.0018	0.185	0.0030	...	...	...	0.0048	0.400	0.0080	-	-	-	-	-	-	2.8
16,17	...	0.75	0.0074	0.267	0.0122	...	...	...	0.0041	0.017	0.0062	-	-	-	-	-	-	2.5
16,17	...	0.75	0.0004	0.178	0.0007	...	...	...	0.0048	0.330	0.0080	-	-	-	-	-	-	1.7
	...	0.90	0.0046	0.263	0.0076	...	...	...	0.0028	0.013	0.0043	-	-	-	-	-	-	2.7
scc	s	0.50	0.0002	0.060	0.0003	0.0600	0.136	0.0812	0.0195	0.040	0.0256	1.212	0.360	0.823	0.029	13.3	10	6.4
	s	0.75	0.0001	0.031	0.0002	0.0306	0.149	0.0471	0.0226	0.023	0.0226	1.363	0.485	0.869	0.009	3.0	60	5.7
	s	0.75	0.0005	0.037	0.0008	0.0370	0.172	0.0568	0.0267	0.027	0.0269	1.472	0.514	0.946	0.012	8.8	30	5.2
	s	0.75	0.0224	0.060	0.0314	0.0600	0.136	0.0812	0.0218	0.030	0.0251	1.592	0.508	1.060	0.024	13.1	10	4.5

TABLE 3—*Continued*

Type/ Fig.	Cont.	Depl.	Spherical silicate			Cylindrical silicate			Carbon			A(V)							
			a_-/a_c	a_+/a_i	$\langle a \rangle$	a_-/a_c	a_+/a_i	$\langle a \rangle$	a_-/a_c	a_+/a_i	$\langle a \rangle$	Total	Carbon	Sp.sil.	Cyl.sil.	$\frac{P(V)}{A(V)}$	γ	χ^2
			(μm)	(μm)	(μm)	(μm)	(μm)	(μm)	(μm)	(μm)	(μm)	(mag)	(mag)	(mag)	(mag)	($\frac{\%}{mag}$)	(°)	
(1)	(2)	(3)	(4)	(5)	(6)	(7)	(8)	(9)	(10)	(11)	(12)	(13)	(14)	(15)	(16)	(17)	(18)	(19)
	s	0.90	0.0001	0.031	0.0002	0.0306	0.149	0.0471	0.0202	0.021	0.0206	1.447	0.569	0.869	0.009	2.8	60	5.0
	s	0.90	0.0003	0.037	0.0005	0.0370	0.172	0.0568	0.0198	0.029	0.0235	1.552	0.599	0.941	0.012	8.3	30	4.4
	s	0.90	0.0276	0.060	0.0369	0.0600	0.136	0.0812	0.0210	0.028	0.0238	1.718	0.596	1.099	0.023	12.6	10	4.3
	v	0.25	0.0075	0.060	0.0120	0.0600	0.136	0.0812	0.0253	0.063	0.0350	0.959	0.246	0.666	0.047	13.6	10	5.4
	v	0.50	0.0092	0.060	0.0144	0.0600	0.136	0.0812	0.0039	0.069	0.0064	1.133	0.419	0.666	0.048	11.5	10	3.8
	v	0.75	0.0015	0.031	0.0025	0.0306	0.149	0.0471	0.0001	0.061	0.0002	1.070	0.495	0.547	0.028	2.4	60	6.4
	v	0.75	0.0008	0.037	0.0013	0.0370	0.172	0.0568	0.0003	0.055	0.0005	1.147	0.524	0.594	0.029	7.1	30	7.4
18	**v**	**0.75**	**0.0127**	**0.060**	**0.0195**	**0.0600**	**0.136**	**0.0812**	**0.0001**	**0.075**	**0.0002**	**1.293**	**0.576**	**0.666**	**0.051**	**10.1**	**10**	**2.7**
	v	0.90	0.0102	0.031	0.0146	0.0306	0.149	0.0471	0.0003	0.065	0.0005	1.260	0.683	0.547	0.030	2.0	60	8.4
	v	0.90	0.0011	0.037	0.0018	0.0370	0.172	0.0568	0.0003	0.046	0.0004	1.156	0.532	0.594	0.030	7.1	30	6.6
	v	0.90	0.0218	0.060	0.0308	0.0600	0.136	0.0812	0.0002	0.109	0.0002	1.677	0.952	0.666	0.059	7.8	10	5.9
ecc	s	0.10	0.0013	0.061	0.0021	0.0608	0.099	0.0746	0.0915	0.127	0.1061	0.569	0.228	0.333	0.008	10.6	30	3.3
	s	0.25	0.0001	0.061	0.0002	0.0608	0.099	0.0746	0.0004	0.279	0.0007	0.623	0.302	0.313	0.008	9.1	30	3.9
	s	0.50	0.0001	0.045	0.0002	0.0455	0.186	0.0686	0.0290	0.029	0.0292	0.934	0.357	0.576	0.001	7.5	30	4.1
18,19	**s**	**0.75**	**0.0001**	**0.045**	**0.0002**	**0.0455**	**0.186**	**0.0686**	**0.0144**	**0.035**	**0.0199**	**1.080**	**0.503**	**0.576**	**0.001**	**6.4**	**30**	**2.4**
18,19	**s**	**0.90**	**0.0023**	**0.045**	**0.0038**	**0.0455**	**0.186**	**0.0686**	**0.0127**	**0.034**	**0.0179**	**1.196**	**0.591**	**0.603**	**0.002**	**6.1**	**30**	**2.4**
	v	0.10	0.0045	0.061	0.0073	0.0608	0.099	0.0746	0.0879	0.112	0.0983	0.591	0.242	0.339	0.010	10.4	30	2.9
	v	0.10	0.0027	0.076	0.0045	0.0765	0.141	0.0978	0.0467	0.047	0.0469	0.534	0.103	0.414	0.017	14.0	10	3.6
	v	0.25	0.0010	0.045	0.0016	0.0455	0.186	0.0686	0.0309	0.058	0.0396	0.625	0.245	0.377	0.003	7.3	30	5.1
	v	0.25	0.0101	0.076	0.0161	0.0765	0.141	0.0978	0.0005	0.111	0.0008	0.718	0.282	0.414	0.022	10.4	10	5.2
	v	0.50	0.0114	0.043	0.0170	0.0427	0.088	0.0564	0.0488	0.170	0.0720	1.212	0.946	0.261	0.005	1.6	60	7.8
	v	0.50	0.0097	0.045	0.0149	0.0455	0.186	0.0686	0.0001	0.084	0.0002	0.808	0.426	0.377	0.005	5.6	30	7.1
	v	0.50	0.0089	0.076	0.0143	0.0765	0.141	0.0978	0.0002	0.021	0.0003	0.677	0.242	0.414	0.021	11.0	10	6.9
	v	0.75	0.0089	0.043	0.0136	0.0427	0.088	0.0564	0.0113	0.136	0.0185	1.338	1.073	0.261	0.004	1.5	60	8.0
	v	0.75	0.0067	0.045	0.0106	0.0455	0.186	0.0686	0.0010	0.068	0.0016	0.980	0.598	0.377	0.005	4.7	30	3.2
	v	0.90	0.0090	0.043	0.0138	0.0427	0.088	0.0564	0.0036	0.136	0.0059	1.435	1.170	0.261	0.004	1.4	60	7.8
	v	0.90	0.0145	0.045	0.0210	0.0455	0.186	0.0686	0.0001	0.171	0.0002	1.474	1.090	0.377	0.007	3.1	30	9.5
sgg	-	0.75	0.0034	0.058	0.0206	0.0243	0.056	0.0407	0.0010	0.104	0.0318	1.789	1.446	0.241	0.102	1.0	60	6.7

TABLE 3—*Continued*

Type/ Fig.	Cont.	Depl.	Spherical silicate			Cylindrical silicate			Carbon			A(V)							
			a_-/a_c (μm)	a_+/a_i (μm)	$\langle a \rangle$ (μm)	a_-/a_c (μm)	a_+/a_i (μm)	$\langle a \rangle$ (μm)	a_-/a_c (μm)	a_+/a_i (μm)	$\langle a \rangle$ (μm)	Total (mag)	Carbon (mag)	Sp.sil. (mag)	Cyl.sil. (mag)	$\frac{P(V)}{A(V)}$ ($\frac{\%}{mag}$)	γ (°)	χ^2
(1)	(2)	(3)	(4)	(5)	(6)	(7)	(8)	(9)	(10)	(11)	(12)	(13)	(14)	(15)	(16)	(17)	(18)	(19)
	-	0.75	0.0044	0.061	0.0224	0.0390	0.061	0.0571	0.0048	0.105	0.0359	1.705	1.502	0.090	0.113	1.1	30	7.5
	-	0.75	0.0045	0.061	0.0230	0.0514	0.079	0.0748	0.0045	0.105	0.0355	1.699	1.497	0.087	0.115	1.0	10	7.6
20	-	**0.90**	**0.0046**	**0.060**	**0.0224**	**0.0243**	**0.056**	**0.0407**	**0.0053**	**0.115**	**0.0393**	**2.261**	**1.910**	**0.241**	**0.110**	**0.8**	**60**	**8.9**
	-	0.90	0.0044	0.062	0.0228	0.0390	0.061	0.0571	0.0029	0.120	0.0383	2.131	1.924	0.090	0.117	0.9	30	9.3
	-	0.90	0.0020	0.066	0.0216	0.0514	0.079	0.0748	0.0037	0.119	0.0389	2.135	1.926	0.087	0.122	0.8	10	9.5
egg/20	-	**0.50**	**0.0009**	**0.038**	**0.0122**	**0.0247**	**0.058**	**0.0420**	**0.0060**	**0.080**	**0.0297**	**1.046**	**0.796**	**0.243**	**0.007**	**1.7**	**60**	**5.1**
	-	0.50	0.0042	0.039	0.0157	0.0509	0.051	0.0659	0.0035	0.080	0.0271	0.867	0.762	0.096	0.009	2.1	30	6.9
	-	0.50	0.0022	0.040	0.0141	0.0688	0.069	0.0893	0.0033	0.079	0.0268	0.859	0.756	0.095	0.008	2.1	10	7.5
								Galaxy										
sgr	s	0.60	0.0200	0.250	0.0326	-	-	-	0.0050	0.250	0.0083	-	-	-	-	-	-	-

NOTE.— Columns: (1) Model type as described below; (2) The continuity adopted: "s", size continuity and "v", volume continuity (see text); (3) Carbon depletion assumed; (4) Minimum size of spherical silicate grains; (5) Maximum size of spherical silicate grains; (6) Average size of the spherical silicate population; (7) Minimum size of cylindrical silicate grains; (8) Maximum size of cylindrical silicate grains; (9) Average size of the cylindrical silicate population; (10) Minimum size of carbon grains; (11) Maximum size of carbon grains; (12) Average size of the carbon population; (13, 14, 15 and 16) Total extinction produced by the model, and the fractions corresponding to carbon, spherical and cilindrical silicate grains, respectively; (17) Polarizing efficiency; (18) Angle between the the magnetic field and the plane of sky; (19) Reduced chi^2 as a parameter of the fit quality.

NOTE.—The entries in bold-face type are plotted in the figures whose numbers are given in column 1.

NOTE.— The types describe the adopted model and represent:

- sgr: spherical astronomical silicate + spherical graphite, MRN model
- egr: spherical enstatite + spherical graphite, MRN model
- sgc: spherical astronomical silicate + cylindrical astronomical silicate + spherical graphite, MRN model
- egc: spherical enstatite + cylindrical enstatite + spherical graphite, MRN model
- sca: spherical astronomical silicate + spherical amorphous carbon, MRN model
- eca: spherical enstatite + spherical amorphous carbon, MRN model
- scc: spherical astronomical silicate + cylindrical astronomical silicate + spherical amorphous carbon, MRN model
- ecc: spherical enstatite + cylindrical enstatite + spherical amorphous carbon, MRN model
- sgg: spherical astronomical silicate + cylindrical astronomical silicate + spherical graphite, CG model
- egg: spherical enstatite + cylindrical enstatite + spherical graphite, CG model

TABLE 4

SIZE PARAMETERS OBTAINED FITTING AZV 456 EXTINCTION CURVE

Type/ Fig. (1)	Cont. (2)	Depl. (3)	Spherical silicate a_-/a_c (μm) (4)	Spherical silicate a_+/a_i (μm) (5)	Spherical silicate $\langle a \rangle$ (μm) (6)	Cylindrical silicate a_-/a_c (μm) (7)	Cylindrical silicate a_+/a_i (μm) (8)	Cylindrical silicate $\langle a \rangle$ (μm) (9)	Carbon a_-/a_c (μm) (10)	Carbon a_+/a_i (μm) (11)	Carbon $\langle a \rangle$ (μm) (12)	A(V) Total (mag) (13)	A(V) Carbon (mag) (14)	A(V) Sp.sil. (mag) (15)	A(V) Cyl.sil. (mag) (16)	$\frac{P(V)}{A(V)}$ (% /mag) (17)	γ (°) (18)	χ^2 (19)
sgr	...	0.10	0.0255	0.254	0.0413	...	...	...	0.0037	0.050	0.0060	-	-	-	-	-	-	7.4
21	**...**	**0.25**	**0.0177**	**0.265**	**0.0290**	**...**	**...**	**...**	**0.0017**	**0.079**	**0.0029**	**-**	**-**	**-**	**-**	**-**	**-**	**1.3**
	...	0.50	0.0158	0.215	0.0259	...	...	...	0.0020	0.180	0.0033	-	-	-	-	-	-	1.4
egr	...	0.10	0.0193	0.298	0.0316	...	...	...	0.0062	0.067	0.0101	-	-	-	-	-	-	1.3
21	**...**	**0.25**	**0.0153**	**0.288**	**0.0253**	**...**	**...**	**...**	**0.0039**	**0.180**	**0.0065**	**-**	**-**	**-**	**-**	**-**	**-**	**0.9**
	...	0.50	0.0149	0.223	0.0244	...	...	...	0.0039	0.466	0.0065	-	-	-	-	-	-	1.1
sgc	s	0.25	0.0276	0.099	0.0409	0.0992	0.131	0.1125	0.0154	0.083	0.0239	0.121	0.037	0.069	0.015	9.7	10	6.9
	s	0.50	0.0196	0.099	0.0303	0.0992	0.131	0.1125	0.0100	0.099	0.0162	0.157	0.078	0.064	0.015	7.0	10	4.0
	s	0.75	0.0172	0.099	0.0270	0.0992	0.131	0.1125	0.0094	0.141	0.0155	0.203	0.127	0.062	0.014	5.2	10	8.4
	v	0.25	0.0246	0.099	0.0371	0.0992	0.131	0.1125	0.0132	0.082	0.0208	0.121	0.036	0.071	0.014	10.0	10	5.7
	v	0.50	0.0032	0.056	0.0052	0.0560	0.160	0.0798	0.0017	0.087	0.0029	0.135	0.062	0.069	0.004	6.0	30	9.8
	v	0.50	0.0160	0.099	0.0251	0.0992	0.131	0.1125	0.0052	0.108	0.0086	0.158	0.075	0.071	0.012	7.6	10	3.6
	v	0.75	0.0279	0.056	0.0365	0.0560	0.160	0.0798	0.0119	0.095	0.0191	0.191	0.116	0.069	0.006	4.3	30	3.3
	v	0.90	0.0314	0.045	0.0365	0.0447	0.145	0.0652	0.0130	0.092	0.0206	0.207	0.139	0.063	0.005	1.2	60	8.0
22	**v**	**0.90**	**0.0266**	**0.056**	**0.0353**	**0.0560**	**0.160**	**0.0798**	**0.0106**	**0.106**	**0.0172**	**0.220**	**0.145**	**0.069**	**0.006**	**3.7**	**30**	**3.2**
egc	s	0.10	0.0168	0.084	0.0260	0.0845	0.200	0.1155	0.0160	0.041	0.0223	0.075	0.009	0.064	0.002	12.3	10	8.0
	s	0.10	0.0268	0.112	0.0406	0.1123	0.145	0.1261	0.0223	0.101	0.0341	0.066	0.018	0.039	0.009	8.8	10	5.0
	s	0.25	0.0017	0.084	0.0028	0.0845	0.200	0.1155	0.0048	0.070	0.0079	0.086	0.028	0.056	0.002	9.4	10	9.3
	s	0.50	0.0231	0.112	0.0356	0.1123	0.145	0.1261	0.0210	0.436	0.0346	0.116	0.069	0.038	0.009	4.9	10	5.7
	v	0.10	0.0224	0.112	0.0346	0.1123	0.145	0.1261	0.0130	0.066	0.0201	0.065	0.012	0.045	0.008	10.3	10	3.1
22	**v**	**0.25**	**0.0174**	**0.112**	**0.0274**	**0.1123**	**0.145**	**0.1261**	**0.0059**	**0.155**	**0.0098**	**0.093**	**0.041**	**0.045**	**0.007**	**7.2**	**10**	**1.5**
	v	0.50	0.0290	0.047	0.0356	0.0472	0.202	0.0717	0.0192	0.097	0.0297	0.127	0.086	0.040	0.001	1.5	60	2.6
22	**v**	**0.50**	**0.0240**	**0.062**	**0.0335**	**0.0619**	**0.192**	**0.0895**	**0.0182**	**0.117**	**0.0288**	**0.136**	**0.091**	**0.043**	**0.002**	**3.1**	**30**	**0.9**
	v	0.50	0.0199	0.084	0.0302	0.0845	0.200	0.1155	0.0200	0.136	0.0317	0.141	0.094	0.043	0.004	4.4	10	6.6
	v	0.75	0.0254	0.047	0.0325	0.0472	0.202	0.0717	0.0163	0.131	0.0261	0.177	0.136	0.040	0.001	0.7	60	1.6
	v	0.75	0.0213	0.062	0.0304	0.0619	0.192	0.0895	0.0156	0.159	0.0252	0.180	0.135	0.043	0.002	2.4	30	5.8
	v	0.90	0.0248	0.047	0.0320	0.0472	0.202	0.0717	0.0156	0.153	0.0252	0.204	0.163	0.040	0.001	0.6	60	3.9

TABLE 4—*Continued*

Type/ Fig.	Cont.	Depl.	Spherical silicate			Cylindrical silicate			Carbon			A(V)						
			a_-/a_c	a_+/a_i	$\langle a \rangle$	a_-/a_c	a_+/a_i	$\langle a \rangle$	a_-/a_c	a_+/a_i	$\langle a \rangle$	Total	Carbon	Sp.sil.	Cyl.sil.	$\frac{P(V)}{A(V)}$	γ	χ^2
			(μm)	(μm)	(μm)	(μm)	(μm)	(μm)	(μm)	(μm)	(μm)	(mag)	(mag)	(mag)	(mag)	(% /mag)	($^\circ$)	
(1)	(2)	(3)	(4)	(5)	(6)	(7)	(8)	(9)	(10)	(11)	(12)	(13)	(14)	(15)	(16)	(17)	(18)	(19)
sgg	...	0.50	0.0051	0.080	0.0287	0.0685	0.023	0.0752	0.0054	0.128	0.0432	0.196	0.116	0.068	0.012	6.0	30	7.0
	...	0.50	0.0057	0.083	0.0302	0.0992	0.039	0.1106	0.0011	0.079	0.0245	0.157	0.076	0.067	0.014	7.5	10	8.0
	...	0.75	0.0202	0.056	0.0369	0.0992	0.039	0.1106	0.0010	0.073	0.0227	0.183	0.105	0.067	0.011	6.5	10	9.1
egg/23	**...**	**0.25**	**0.0047**	**0.060**	**0.0225**	**0.1181**	**0.028**	**0.1265**	**0.0048**	**0.049**	**0.0192**	**0.101**	**0.025**	**0.075**	**0.001**	**11.4**	**10**	**2.9**

TABLE 4—*Continued*

Type/ Fig.	Cont.	Depl.	Spherical silicate			Cylindrical silicate			Carbon			A(V)						
			a_-/a_c (μm)	a_+/a_i (μm)	$\langle a \rangle$ (μm)	a_-/a_c (μm)	a_+/a_i (μm)	$\langle a \rangle$ (μm)	a_-/a_c (μm)	a_+/a_i (μm)	$\langle a \rangle$ (μm)	Total (mag)	Carbon (mag)	Sp.sil. (mag)	Cyl.sil. (mag)	$\frac{P(V)}{A(V)}$ (% /mag)	γ (°)	χ^2
(1)	(2)	(3)	(4)	(5)	(6)	(7)	(8)	(9)	(10)	(11)	(12)	(13)	(14)	(15)	(16)	(17)	(18)	(19)
								Galaxy										
sgr	s	0.60	0.0200	0.250	0.0326	-	-	-	0.0050	0.250	0.0083	-	-	-	-	-	-	-

NOTE.— Columns: (1) Model type as described below; (2) The continuity adopted: "s", size continuity and "v", volume continuity (see text); (3) Carbon depletion assumed; (4) Minimum size of spherical silicate grains; (5) Maximum size of spherical silicate grains; (6) Average size of the spherical silicate population; (7) Minimum size of cylindrical silicate grains; (8) Maximum size of cylindrical silicate grains; (9) Average size of the cylindrical silicate population; (10) Minimum size of carbon grains; (11) Maximum size of carbon grains; (12) Average size of the carbon population; (13, 14, 15 and 16) Total extinction produced by the model, and the fractions corresponding to carbon, spherical and cilindrical silicate grains, respectively; (17) Polarizing efficiency; (18) Angle between the the magnetic field and the plane of sky; (19) Reduced χ^2 as a parameter of the fit quality.

NOTE.—The entries in bold-face type are plotted in the figures whose numbers are given in column 1.

NOTE.— The types describe the adopted model and represent:

- sgr: spherical astronomical silicate + spherical graphite, MRN model
- egr: spherical enstatite + spherical graphite, MRN model
- sgc: spherical astronomical silicate + cylindrical astronomical silicate + spherical graphite, MRN model
- egc: spherical enstatite + cylindrical enstatite + spherical graphite, MRN model
- sca: spherical astronomical silicate + spherical amorphous carbon, MRN model
- eca: spherical enstatite + spherical amorphous carbon, MRN model
- scc: spherical astronomical silicate + cylindrical astronomical silicate + spherical amorphous carbon, MRN model
- ecc: spherical enstatite + cylindrical enstatite + spherical amorphous carbon, MRN model
- sgg: spherical astronomical silicate + cylindrical astronomical silicate + spherical graphite, CG model
- egg: spherical enstatite + cylindrical enstatite + spherical graphite, CG model

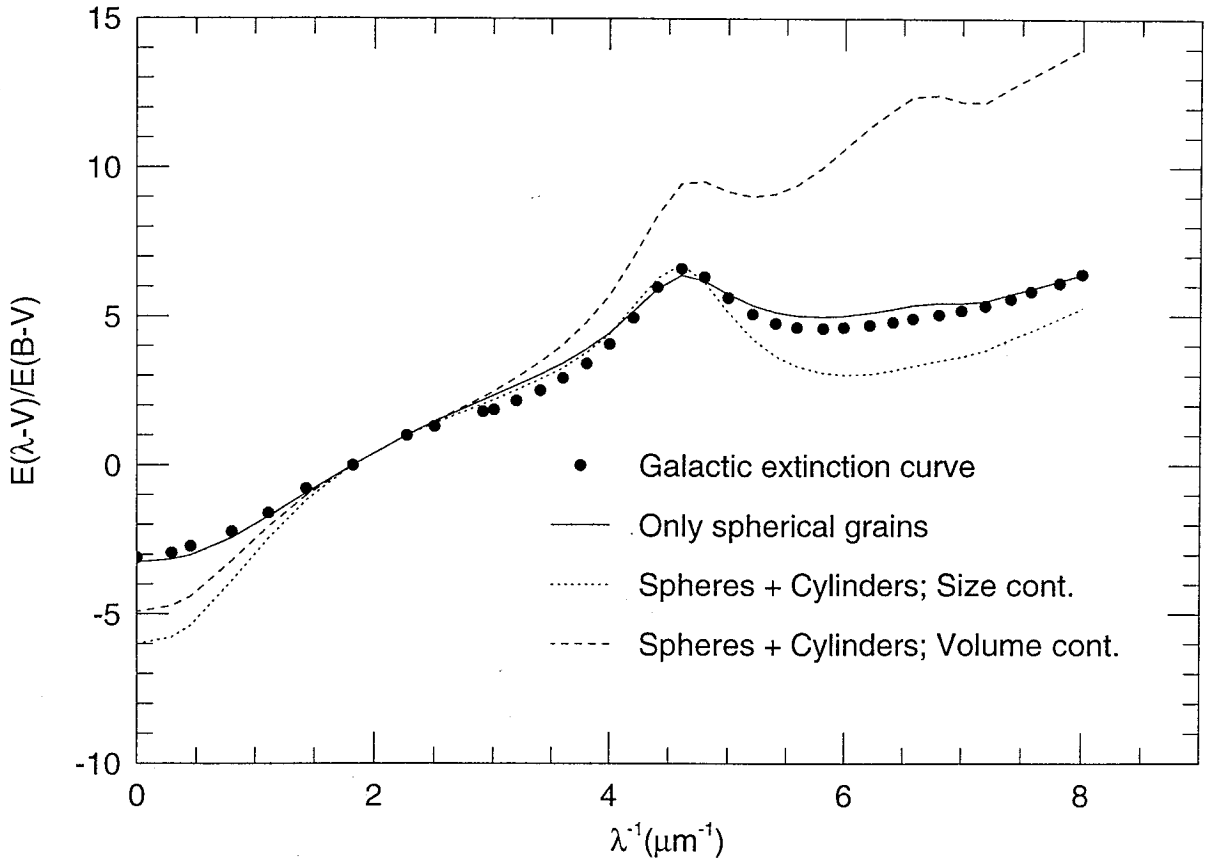

Fig. 1.— Comparison between extinction curves in the MRN model using spherical grains only and using spheres plus cylinders with size continuity and with volume continuity. The size ranges are the same for the three curves, namely, $a_-^{sil} = 0.02\mu$m, $a_+^{sil} = 0.25\mu$m, $a_-^{car} = 0.005\mu$m and $a_+^{car} = 0.25\mu$m. The smallest cylindrical size, a_p^{sil} (=0.055μm), allows the fit to the Galactic polarization curve (in the size and volume continuity curves). The mean Galactic curve is also shown. See Sec. 2.1.1.

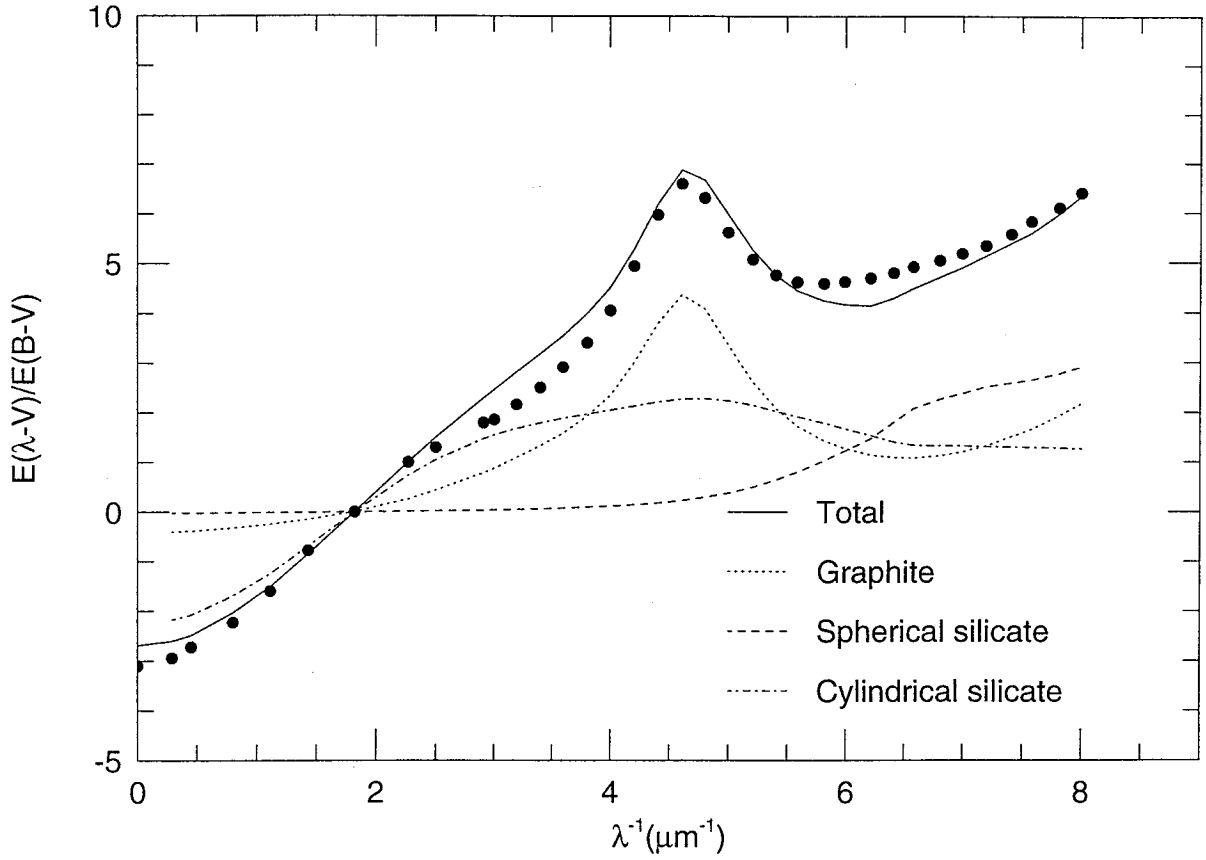

Fig. 2.— A typical extinction curve and its components. The parameters used are $a_{-}^{sil} = 0.001\mu$m, $a_{p}^{sil} = 0.04\mu$m, $a_{+}^{sil} = 0.19\mu$m, $a_{-}^{car} = 0.001\mu$m and $a_{+}^{car} = 0.05\ \mu$m. We have used size continuity, astronomical silicate and $\gamma = 60^{o}$. One should note: (1) the saturation of the extinction of the cylindrical grains in the UV; (2) that the spherical silicate grains are the principal cause of the extinction in the FUV; (3) that graphite makes an important contribution to the FUV rise and a moderate one to the IR extinction.

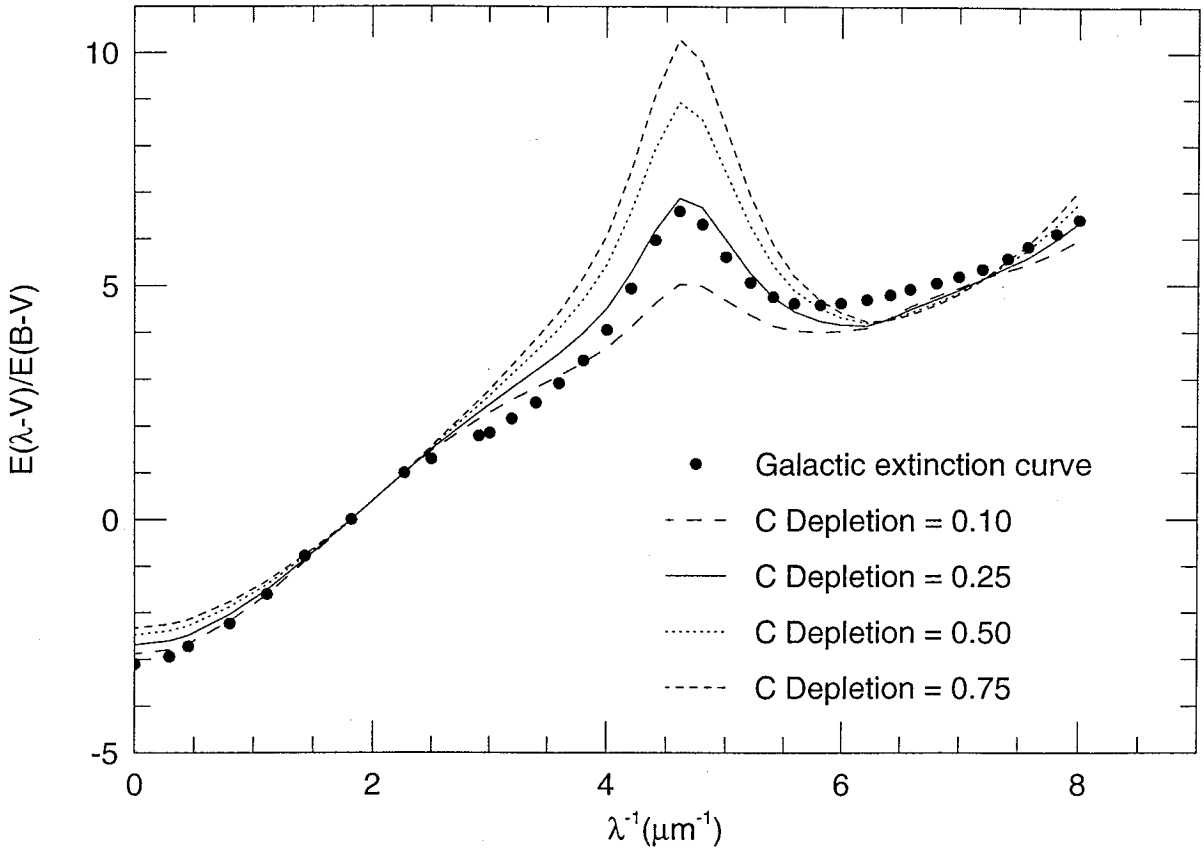

Fig. 3.— Extinction curves using different values of the C depletion. The curves correspond to the values of 0.10, 0.25, 0.50 and 0.75. The dots represent the mean Galactic extinction curve. The size parameters are: $a_{-}^{sil} = 0.001\mu$m, $a_{p}^{sil} = 0.04\mu$m, $a_{+}^{sil} = 0.19\mu$m, $a_{-}^{car} = 0.001\mu$m and $a_{+}^{car} = 0.05\mu$m.

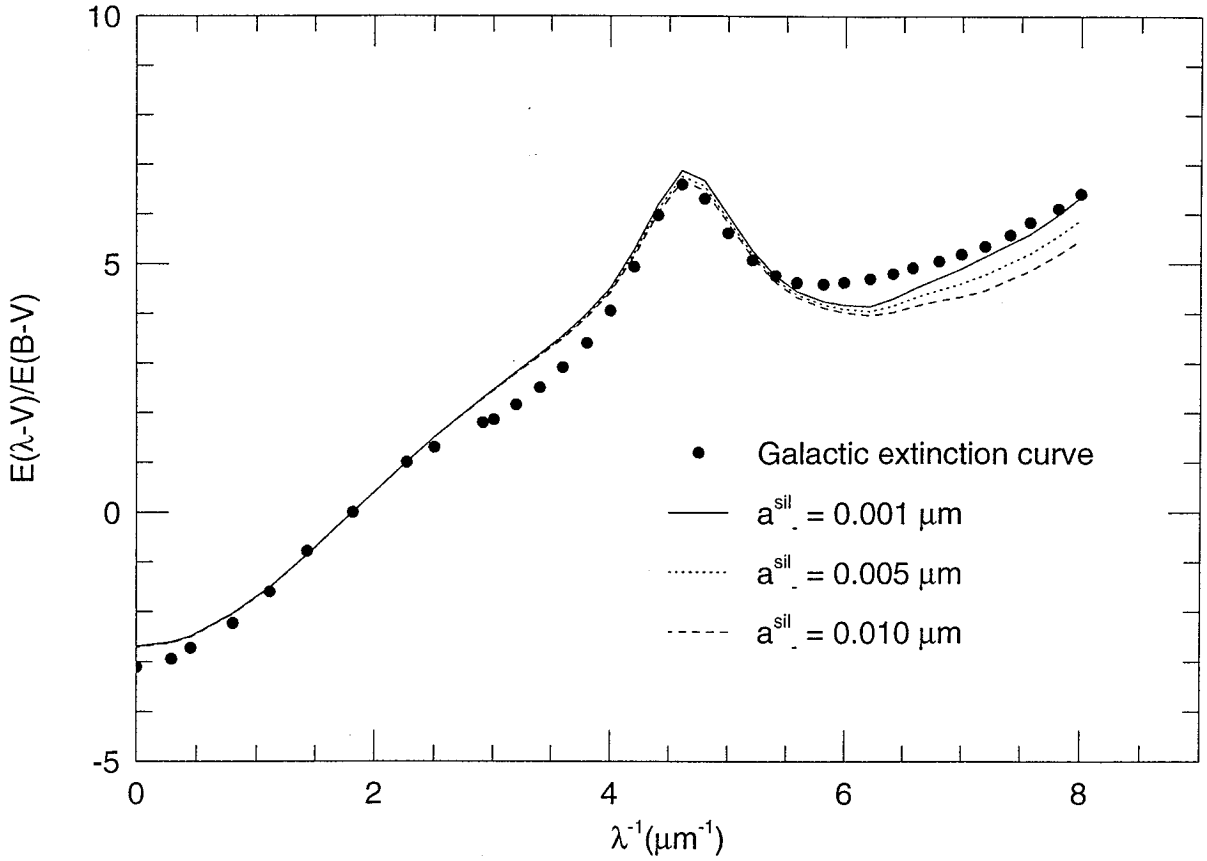

Fig. 4.— Extinction curves using different values of a_{-}^{sil} (size of the smallest silicate spherical grain). The curves correspond to the values of 0.001μm, 0.005μm and 0.01μm. The dots represent the mean Galactic extinction curve. The other size parameters are: $a_{p}^{sil} = 0.04\mu$m, $a_{+}^{sil} = 0.19\mu$m, $a_{-}^{car} = 0.001\mu$m and $a_{+}^{car} = 0.05\mu$m.

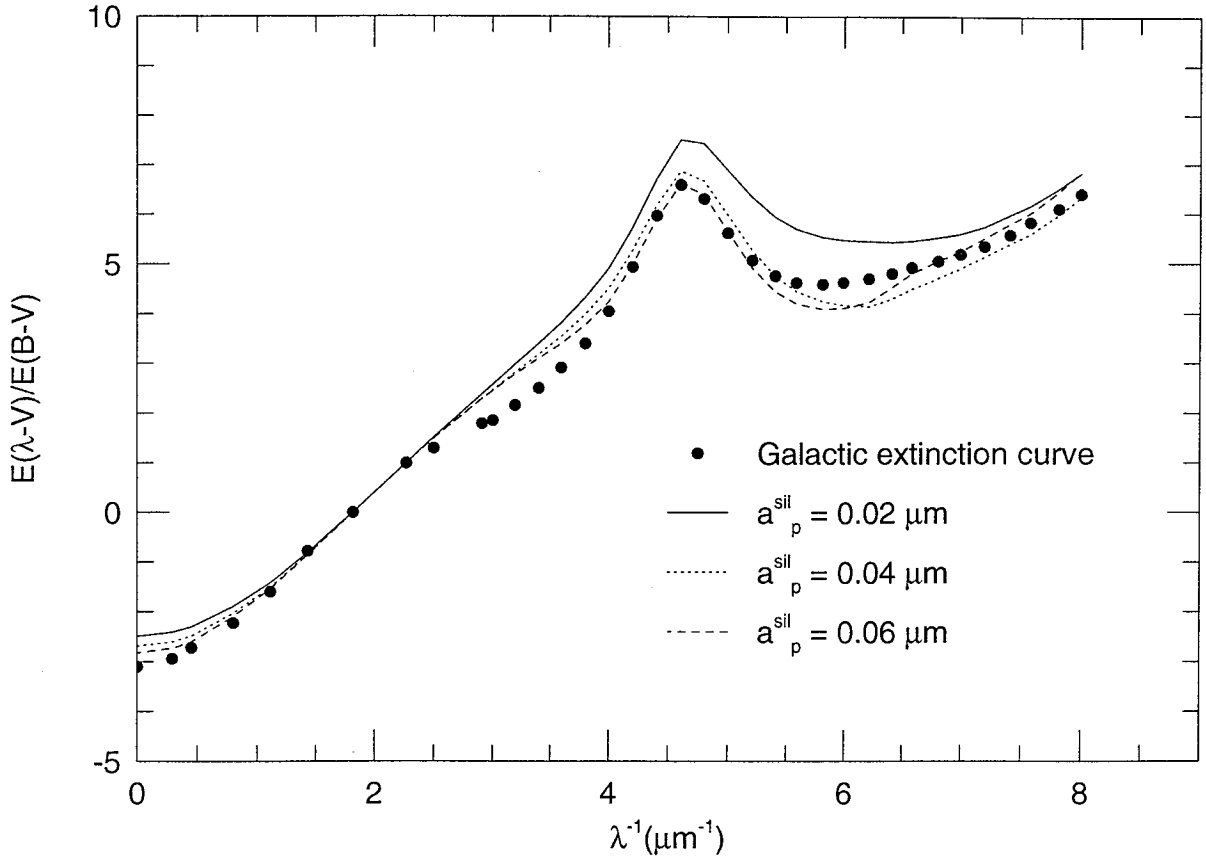

Fig. 5.— Extinction curves using different values of a_p^{sil} (size of the largest silicate spherical grain) which is the same as that of the smallest silicate cylindrical grain). The curves correspond to the values of 0.02μm, 0.04μm and 0.06μm. The greatest differences are found in the UV part of the curve. The dots represent the mean Galactic extinction curve. The other size parameters are: a_-^{sil} = 0.001μm, a_+^{sil} = 0.19μm, a_-^{car} = 0.001μm and a_+^{car} = 0.05μm.

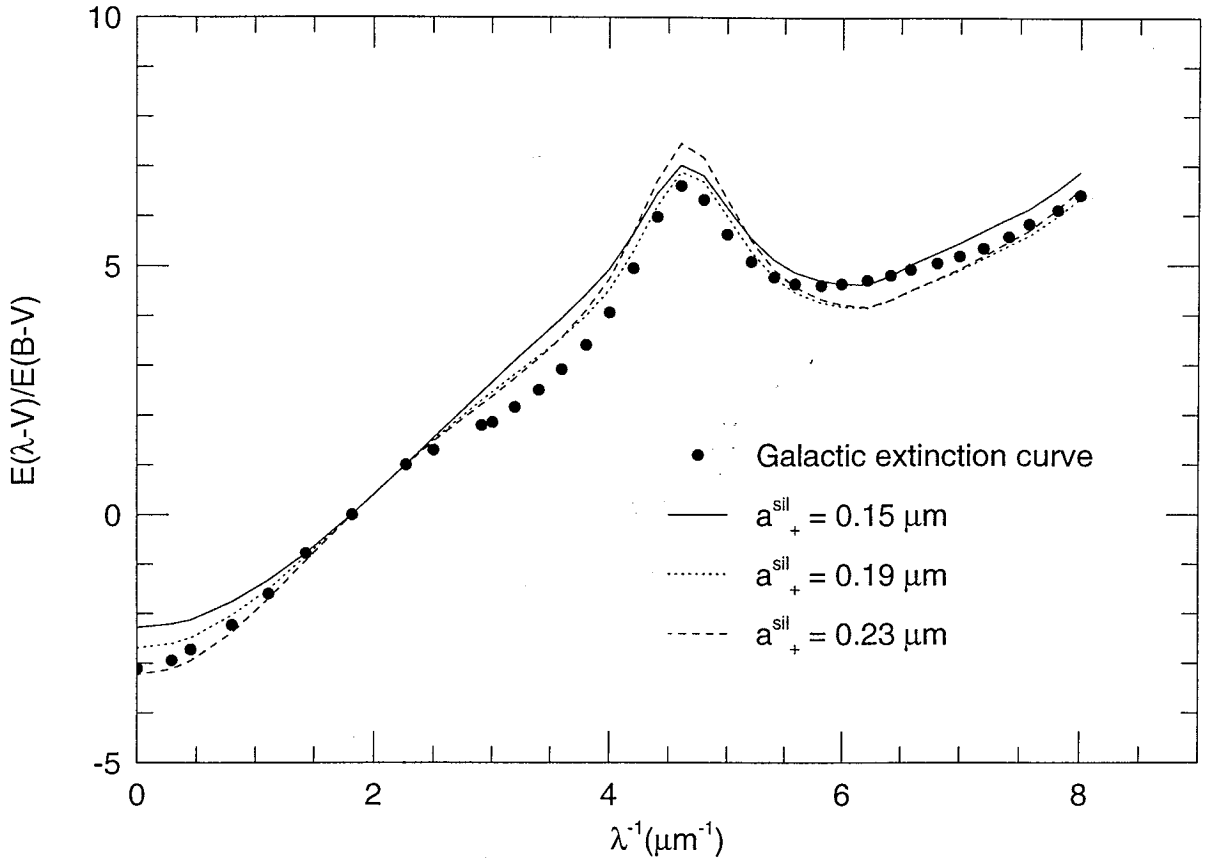

Fig. 6.— Extinction curves using different values of a_+^{sil} (size of the largest silicate cylindrical grain). The curves correspond to the values of 0.15μm, 0.19μm and 0.23μm. The dots represent the mean Galactic extinction curve. The other size parameters are: $a_-^{sil} = 0.001\mu$m, $a_p^{sil} = 0.04\mu$m, $a_-^{car} = 0.001\mu$m and $a_+^{car} = 0.05\mu$m.

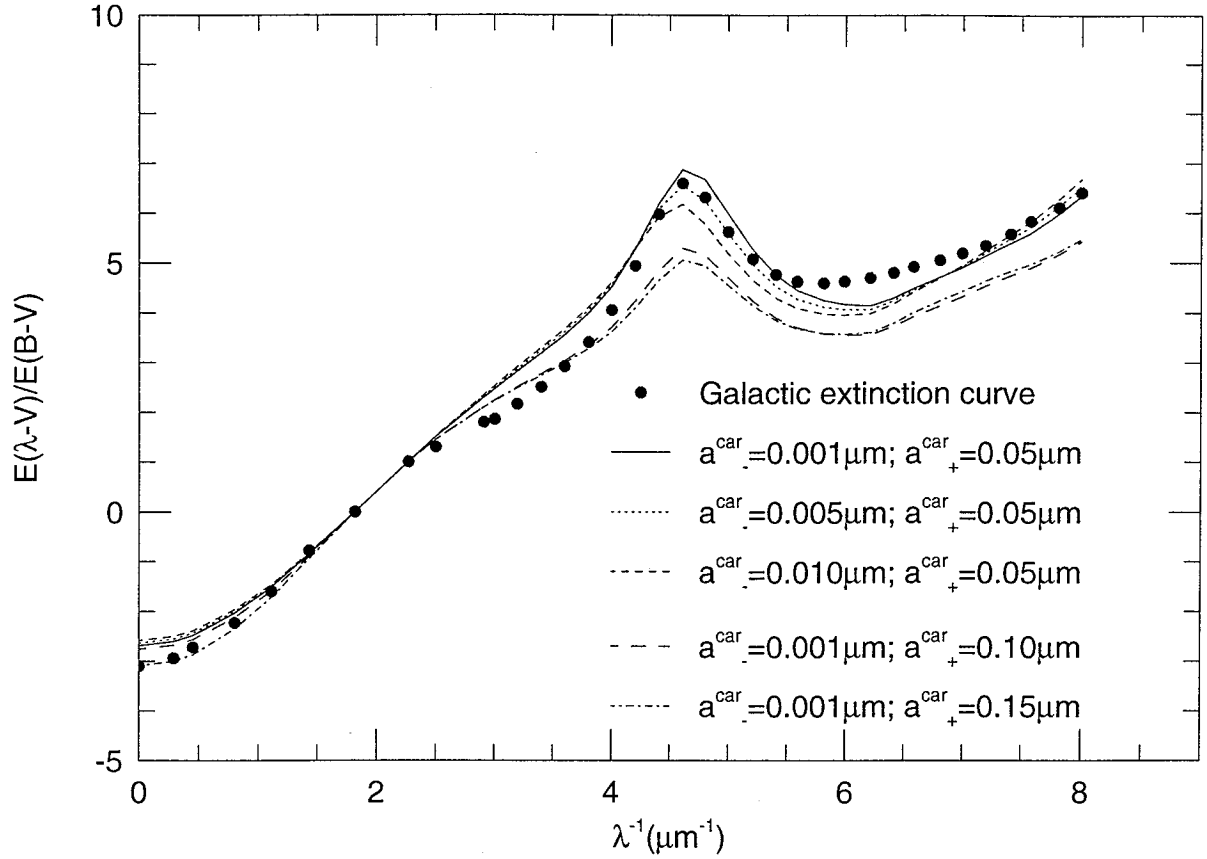

Fig. 7.— Extinction curves using different values of a_-^{car} (size of the smallest graphite grain) and a_+^{car} (size of the largest graphite grain). The values of a_-^{car} are: 0.001μm, 0.005μm and 0.010μm. The values of a_+^{car} are: 0.05μm, 0.10μm and 0.15μm. The dots represent the mean Galactic extinction curve. The silicate sizes are: $a_-^{sil} = 0.001\mu$m, $a_p^{sil} = 0.04\mu$m and $a_+^{sil} = 0.19\mu$m.

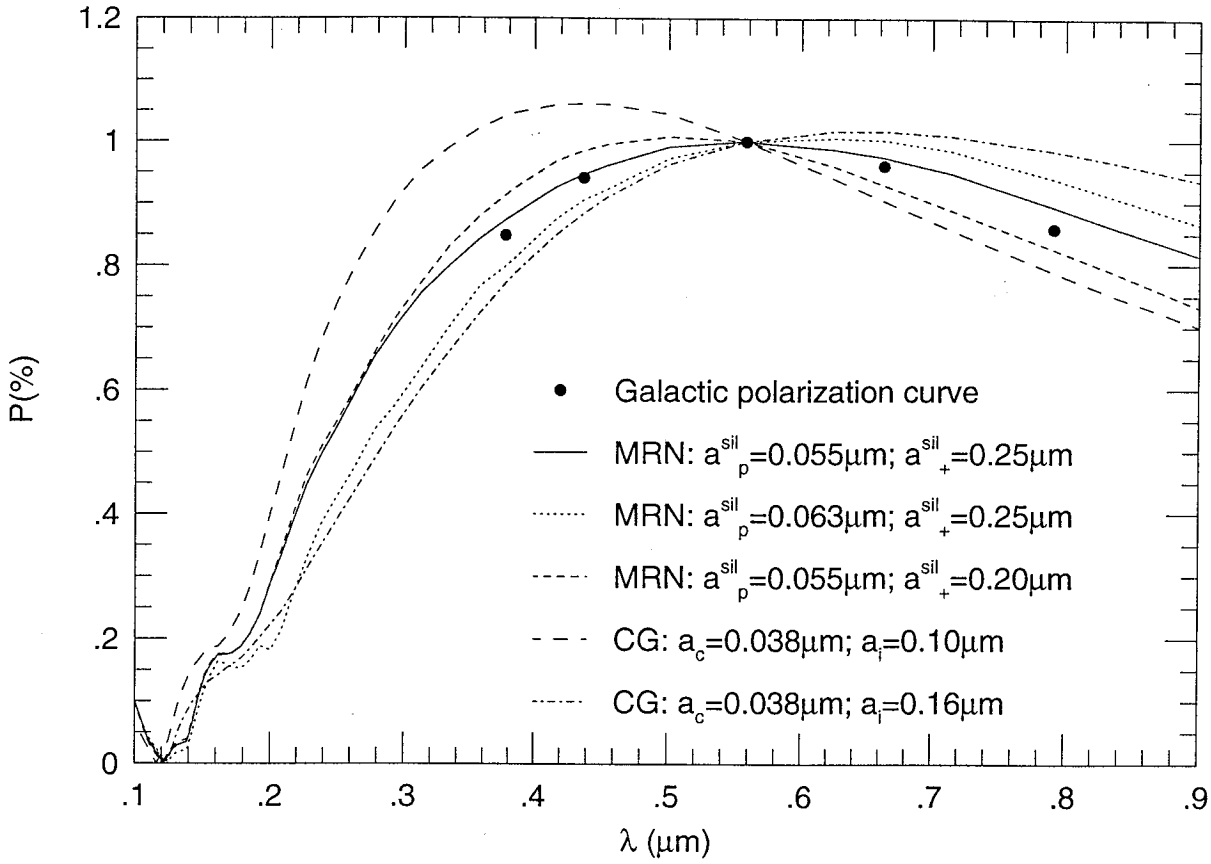

Fig. 8.— Polarization curves obtained for different models and grain sizes. All curves are for a value of $\gamma = 10°$. The points represent a typical Galactic polarization curve. See text (sec. 2.1.2 and 2.2) for more details.

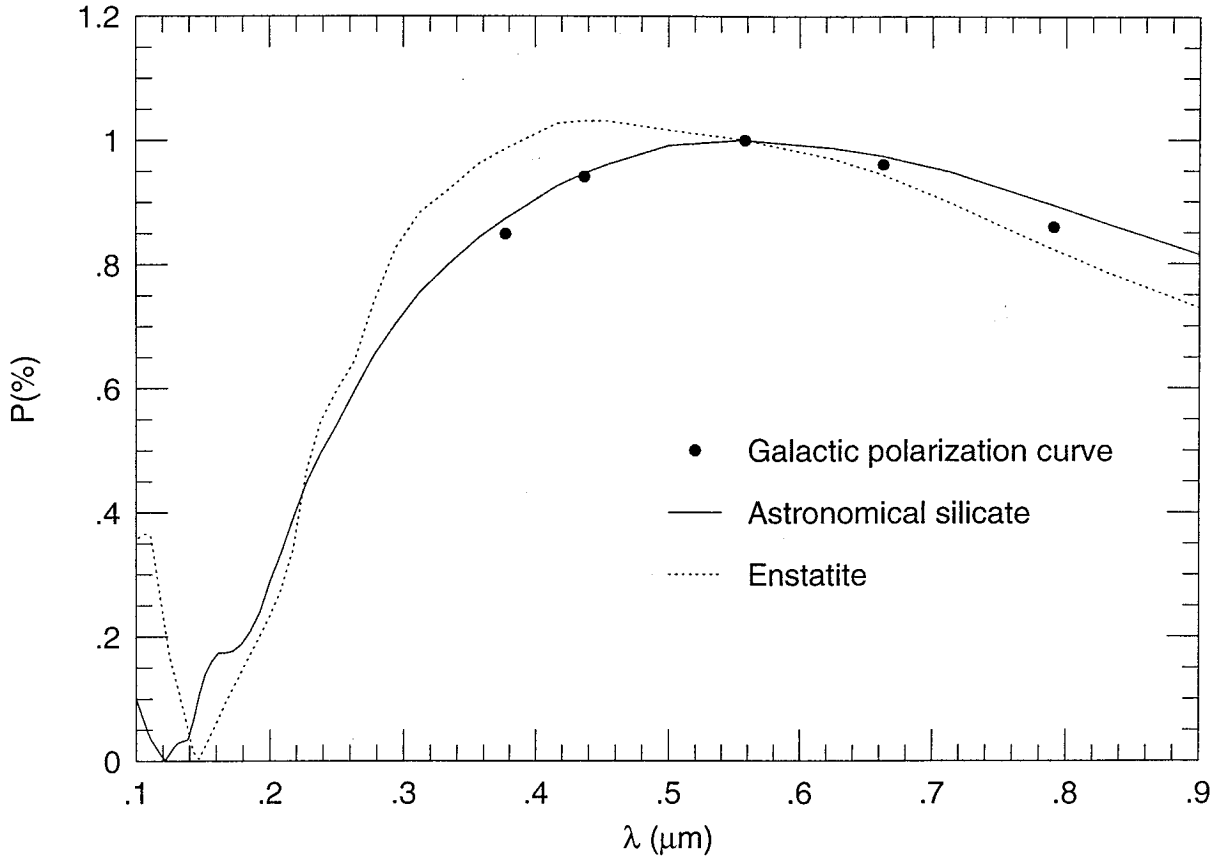

Fig. 9.— Polarization curves using indices of refraction of astronomical silicate and enstatite and the MRN model. The enstatite curve is similar to a curve produced by smaller astronomical silicate grains. The points represent a typical Galactic polarization curve. The sizes used in the models are: $a_p^{sil} = 0.055\mu$m and $a_+^{sil} = 0.25\mu$m.

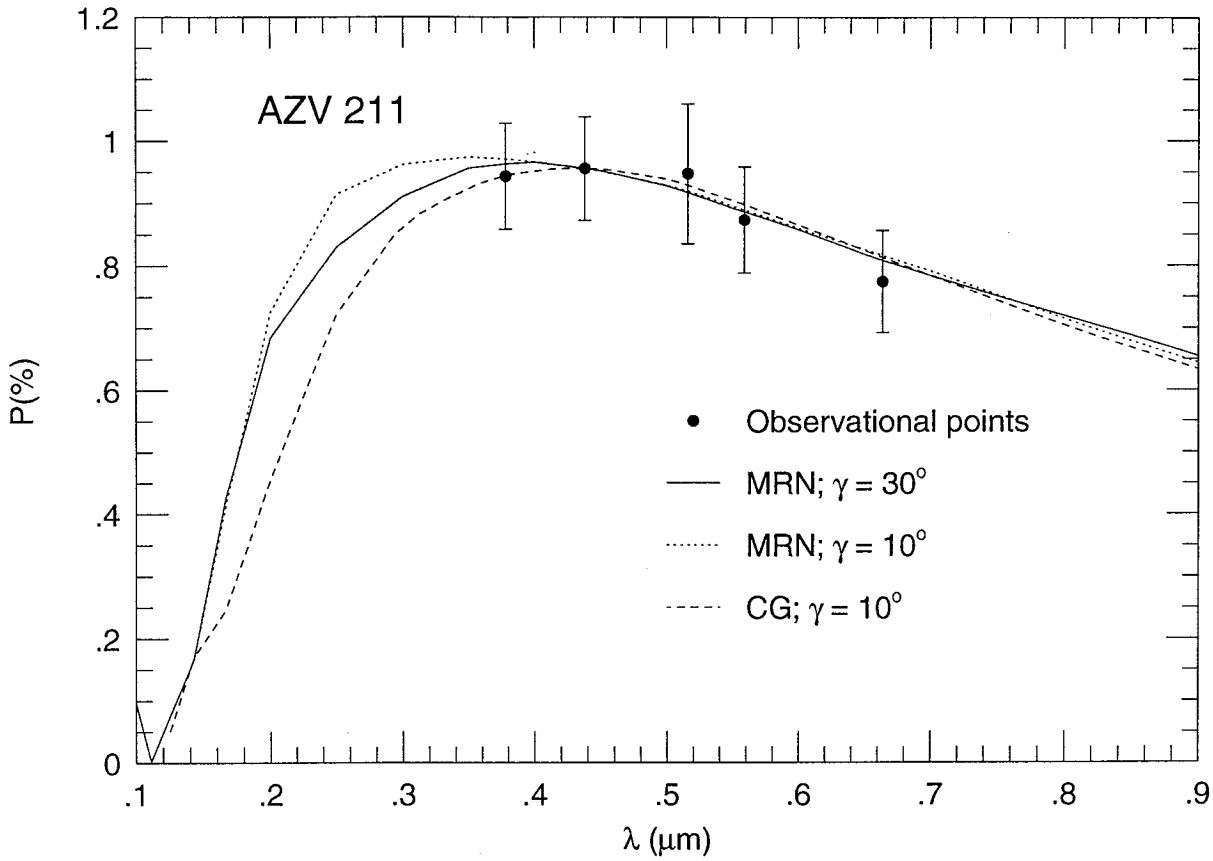

Fig. 10.— Fits to the polarization data of AZV211 using the MRN and CG models. The size distribution parameters used in the models are: $a_p^{sil} = 0.032\mu$m and $a_+^{sil} = 0.235\mu$m (**solid line**); $a_p^{sil} = 0.035\mu$m and $a_+^{sil} = 0.25\mu$m (**dotted line**) and $a_c = 0.030\mu$m and $a_i = 0.106\mu$m (**dashed line**).

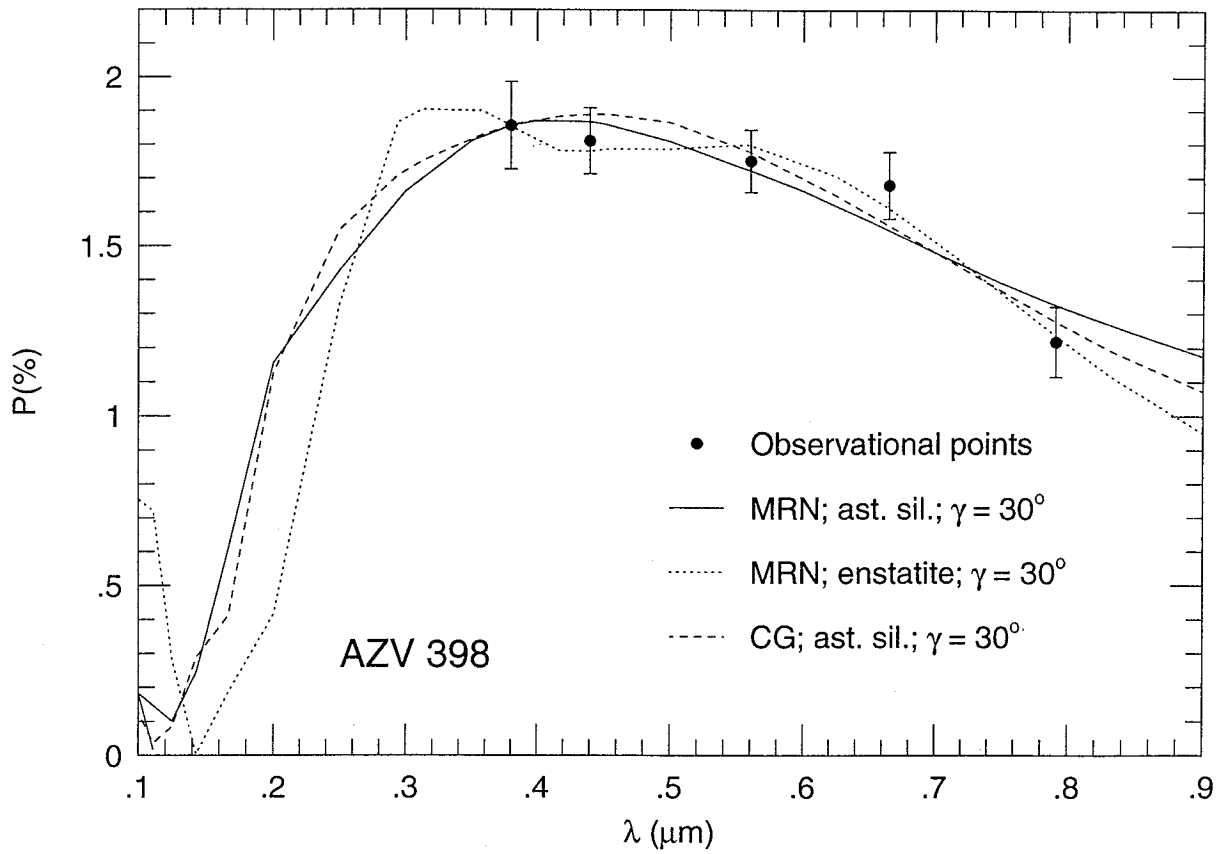

Fig. 11.— Fits to the polarization data of AZV398 using the MRN and CG models. The size distribution parameters used in the models are: $a_p^{sil} = 0.037\mu$m and $a_+^{sil} = 0.172\mu$m (**solid line**); $a_p^{sil} = 0.045\mu$m and $a_+^{sil} = 0.186\mu$m(**dotted line**) and $a_c = 0.039\mu$m and $a_i = 0.061\mu$m (**dashed line**).

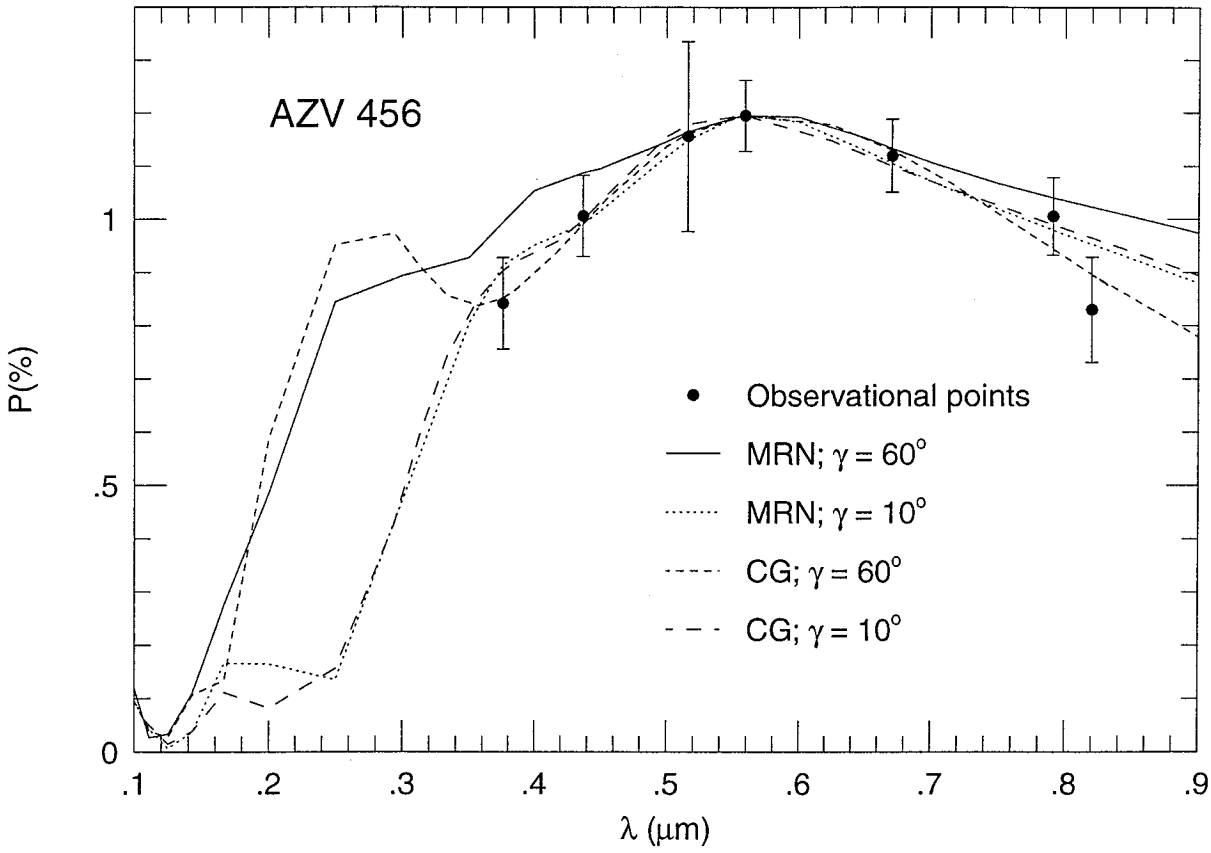

Fig. 12.— Fits to the polarization data of AZV456 using different models and values of γ. Note the broad curve for the MRN model with $\gamma = 60^o$ (**solid line**) and the UV bump in the CG model with $\gamma = 60^o$ (**short-dashed line**). For $\gamma = 10^o$, both models produce almost the same results. The size distribution parameters used in the models are: $a_p^{sil} = 0.045\mu$m and $a_+^{sil} = 0.145\mu$m (**solid line**); $a_p^{sil} = 0.099\mu$m and $a_+^{sil} = 0.131\mu$m (**dotted line**); $a_c = 0.049\mu$m and $a_i = 0.034\mu$m (**short-dashed line**) and $a_c = 0.099\mu$m and $a_i = 0.039\mu$m (**long-dashed line**).

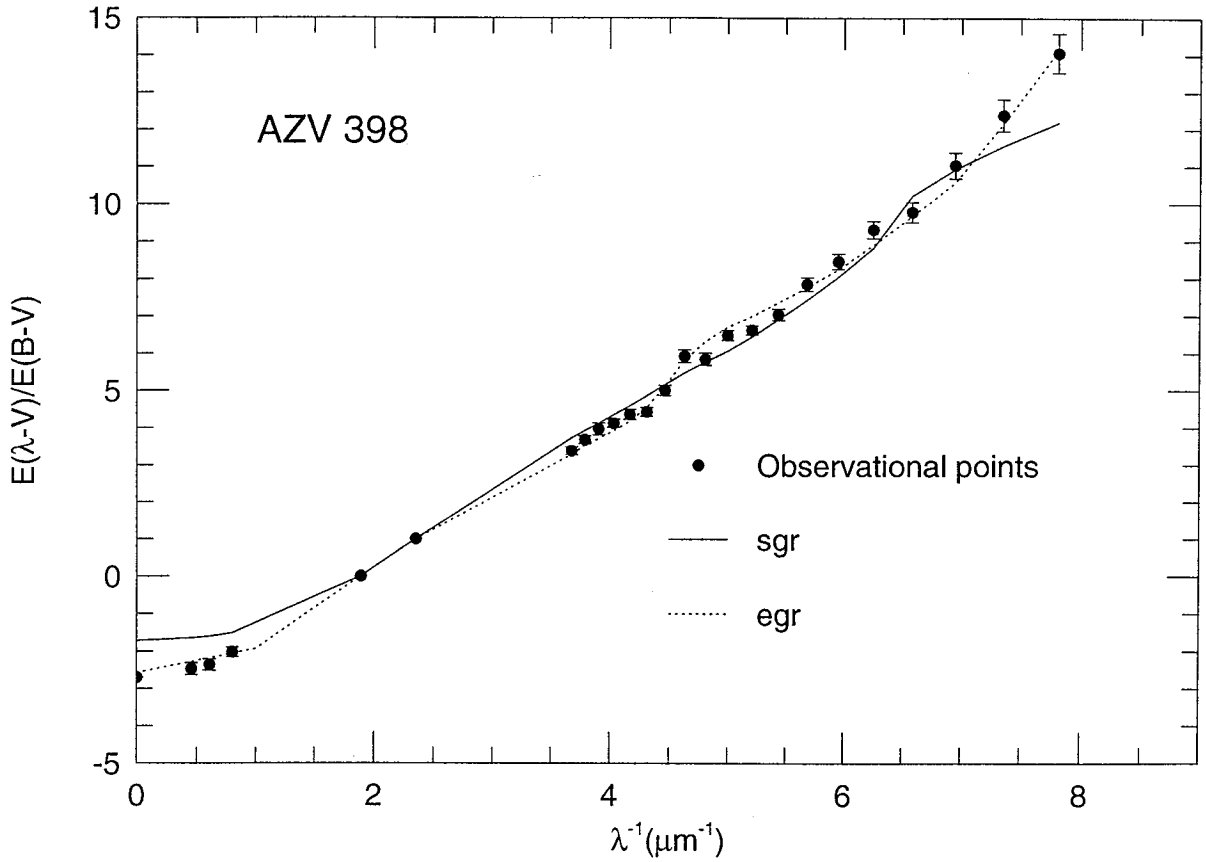

Fig. 13.— Fits to the extinction data of AZV398 using the MRN model with only spherical particles of graphite and silicate. The amount of carbon locked up in the grains is 5% for both curves. Note the better fit in the IR and FUV when using enstatite. The size distribution parameters used in the models are: $a_{-}^{sil} = 0.00099\mu$m, $a_{p}^{sil} = 0.172\mu$m, $a_{-}^{car} = 0.00486\mu$m and $a_{+}^{car} = 0.202\mu$m (**solid line**) and $a_{-}^{sil} = 0.00062\mu$m, $a_{p}^{sil} = 0.290\mu$m, $a_{-}^{car} = 0.00513\mu$m and $a_{+}^{car} = 0.203\mu$m (**dotted line**).

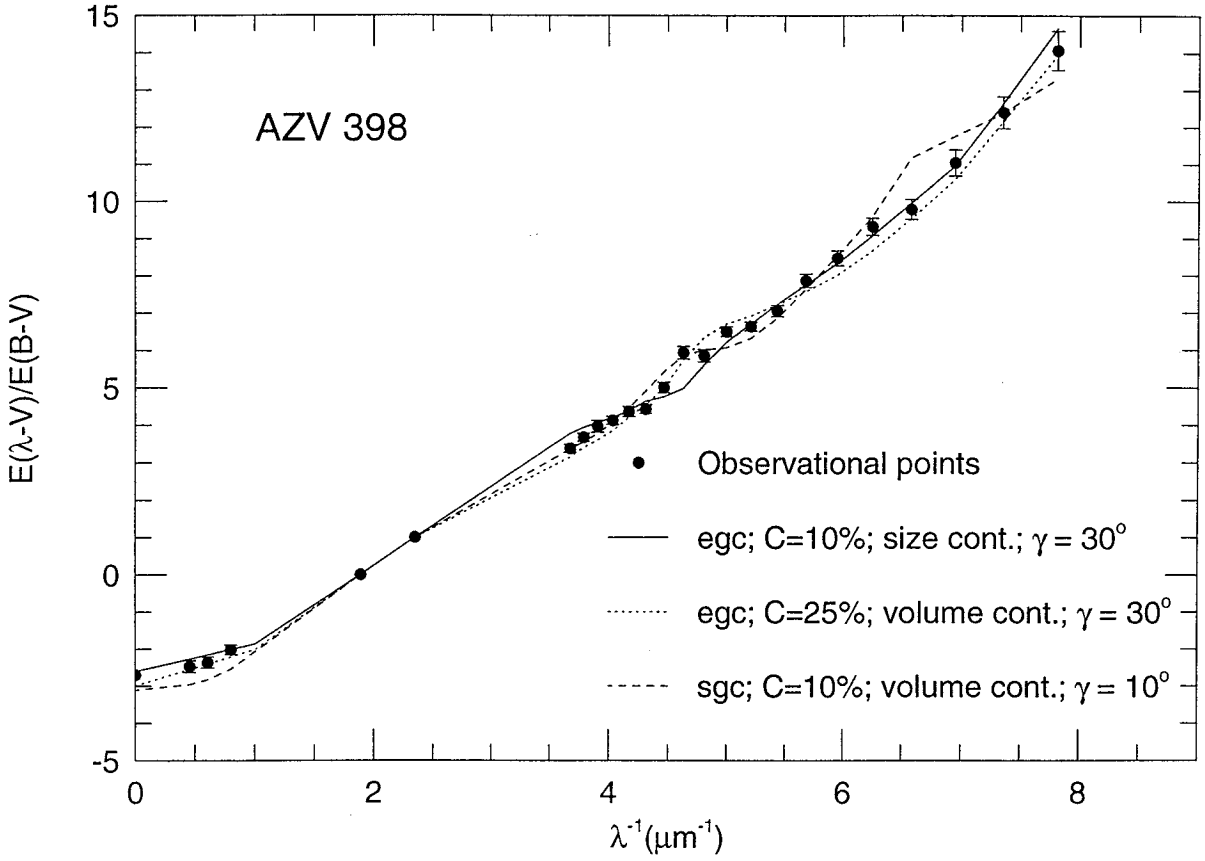

Fig. 14.— Fits to the extinction data of AZV398 using the MRN model with spherical particles of graphite and silicate and cylindrical silicate particles of sizes adjusted by the polarization fits. The maximum size of the spherical silicate particles have been constrained by the distribution for cylindrical particles. The size distribution parameters used in the models are: $a_{-}^{sil} = 0.00077\mu$m, $a_{p}^{sil} = 0.061\mu$m, $a_{+}^{sil} = 0.099\mu$m, $a_{-}^{car} = 0.071\mu$m and $a_{+}^{car} = 0.156\mu$m (**solid line**); $a_{-}^{sil} = 0.01\mu$m, $a_{p}^{sil} = 0.045\mu$m, $a_{+}^{sil} = 0.186\mu$m, $a_{-}^{car} = 0.015\mu$m and $a_{+}^{car} = 0.156\mu$m (**dotted line**) and $a_{-}^{sil} = 0.0060\mu$m, $a_{p}^{sil} = 0.060\mu$m, $a_{+}^{sil} = 0.136\mu$m, $a_{-}^{car} = 0.0046\mu$m and $a_{+}^{car} = 0.074\mu$m (**dashed line**). See text (sec. 3.3.1) for more details.

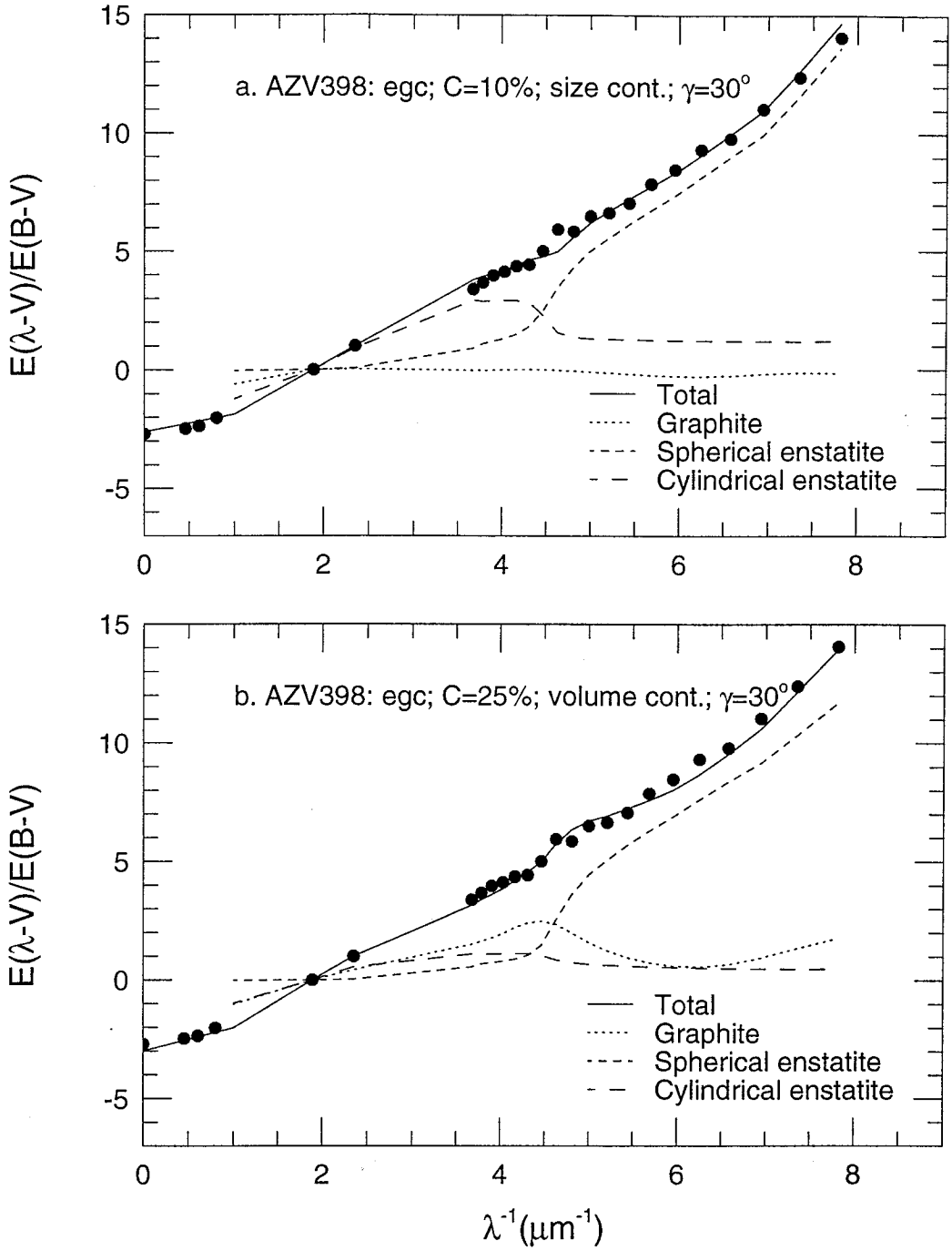

Fig. 15.— Two of the fits to the extinction data of AZV398 shown in Fig. 14. The contribution of each component to each of the extinction fits is shown. See caption to Fig. 14 and the text (sec. 3.3.1) for more details.

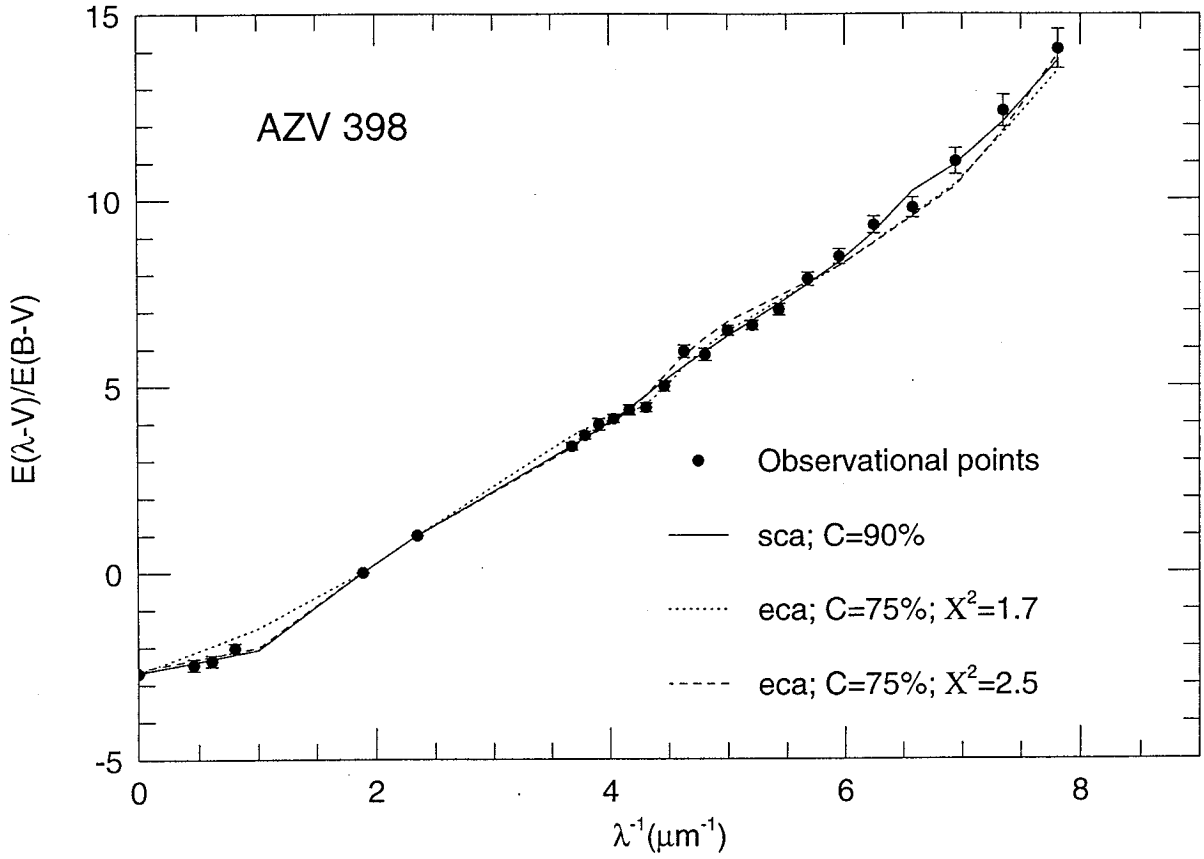

Fig. 16.— Fits to the extinction data of AZV398 using the MRN model with only spherical amorphous carbon and silicate particles. The difference between the two curves using enstatite is due to the differences in size. The size distribution parameters used in the models are: $a_{-}^{sil} = 0.0078\mu$m, $a_{+}^{sil} = 0.228\mu$m, $a_{-}^{car} = 0.0061\mu$m and $a_{+}^{car} = 0.20\mu$m (**solid line**); $a_{-}^{sil} = 0.00043\mu$m, $a_{+}^{sil} = 0.18\mu$m, $a_{-}^{car} = 0.0048\mu$m and $a_{+}^{car} = 0.33\mu$m (**dotted line**) and $a_{-}^{sil} = 0.0074\mu$m, $a_{+}^{sil} = 0.267\mu$m, $a_{-}^{car} = 0.0041\mu$m and $a_{+}^{car} = 0.017\mu$m (**dashed line**). See text (sec. 3.3.1) for more details.

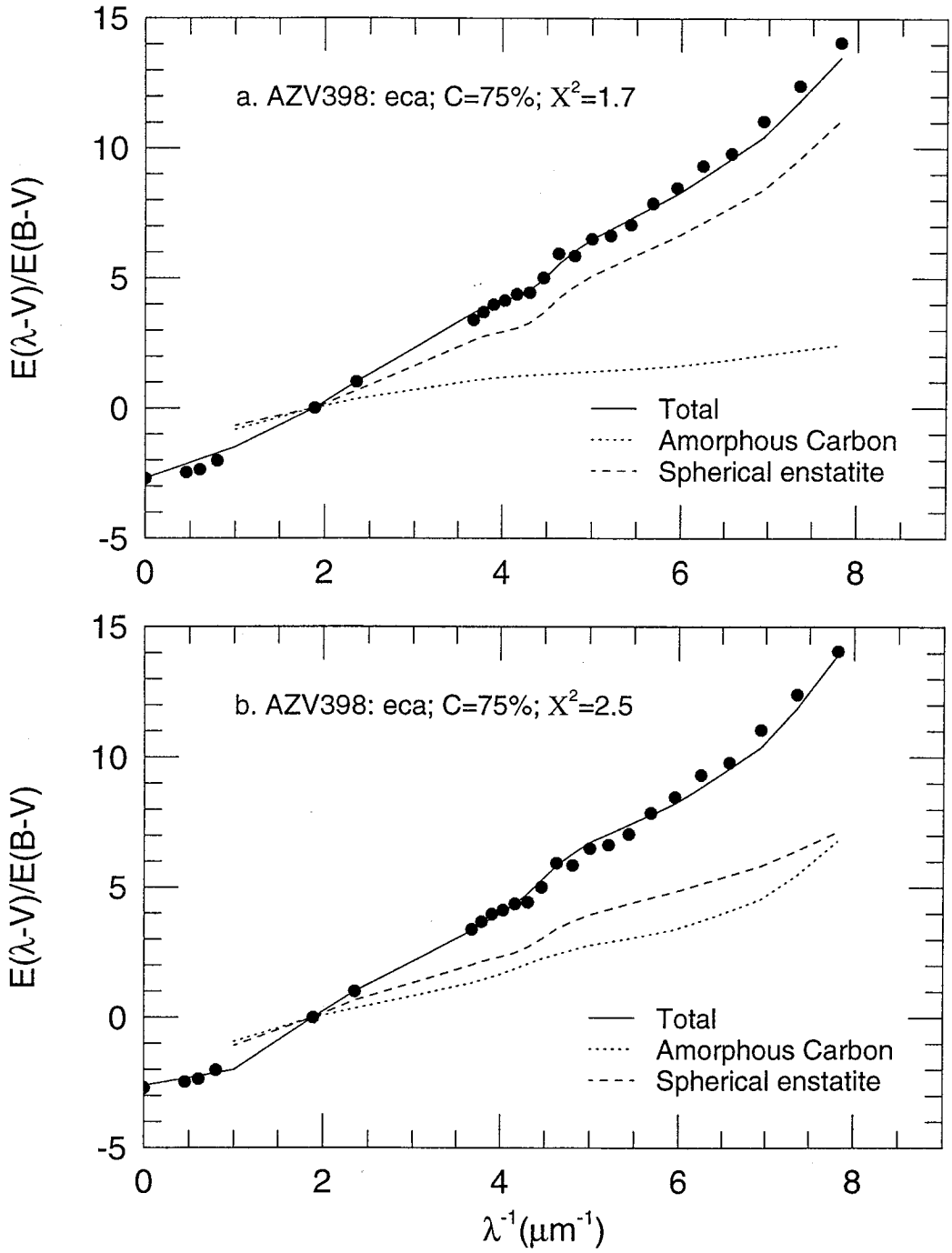

Fig. 17.— Two of the fits to the extinction data of AZV398 shown in Fig. 16. The contribution of each component to each of the extinction fits is shown. See caption to Fig. 16 and the text (sec. 3.3.1) for more details.

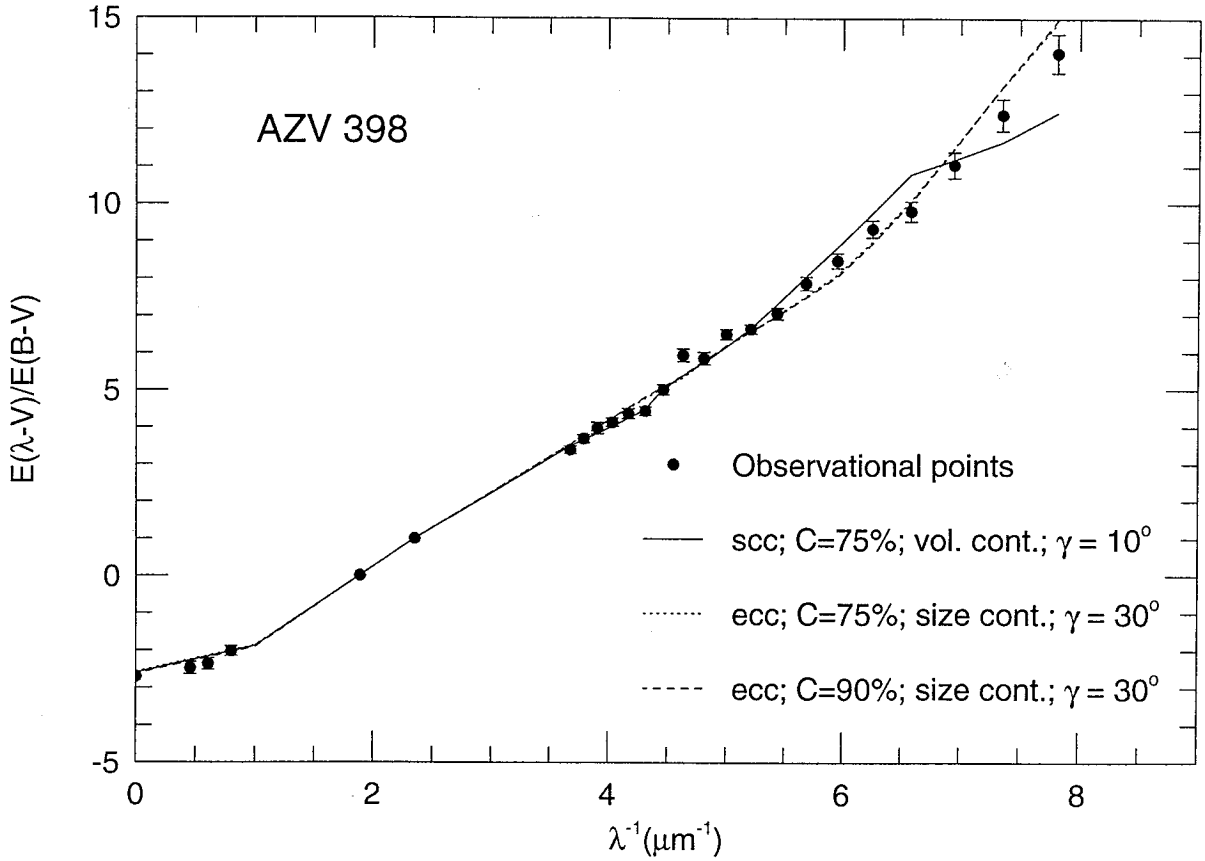

Fig. 18.— Fits to the extinction data of AZV398 using the MRN model with spherical particles of amorphous carbon and spherical and cylindrical silicate grains. Note the better fit obtained when using enstatite. The size distribution parameters used in the models are: $a_{-}^{sil} = 0.013\mu$m, $a_{p}^{sil} = 0.060\mu$m, $a_{+}^{sil} = 0.136\mu$m, $a_{-}^{car} = 0.00011\mu$m and $a_{+}^{car} = 0.075\mu$m (**solid line**); $a_{-}^{sil} = 0.00010\mu$m, $a_{p}^{sil} = 0.045\mu$m, $a_{+}^{sil} = 0.186\mu$m, $a_{-}^{car} = 0.014\mu$m and $a_{+}^{car} = 0.035\mu$m (**dotted line**) and $a_{-}^{sil} = 0.0023\mu$m, $a_{p}^{sil} = 0.045\mu$m, $a_{+}^{sil} = 0.186\mu$m, $a_{-}^{car} = 0.013\mu$m and $a_{+}^{car} = 0.034\mu$m (**dashed line**). See text (sec. 3.3.1) for more details.

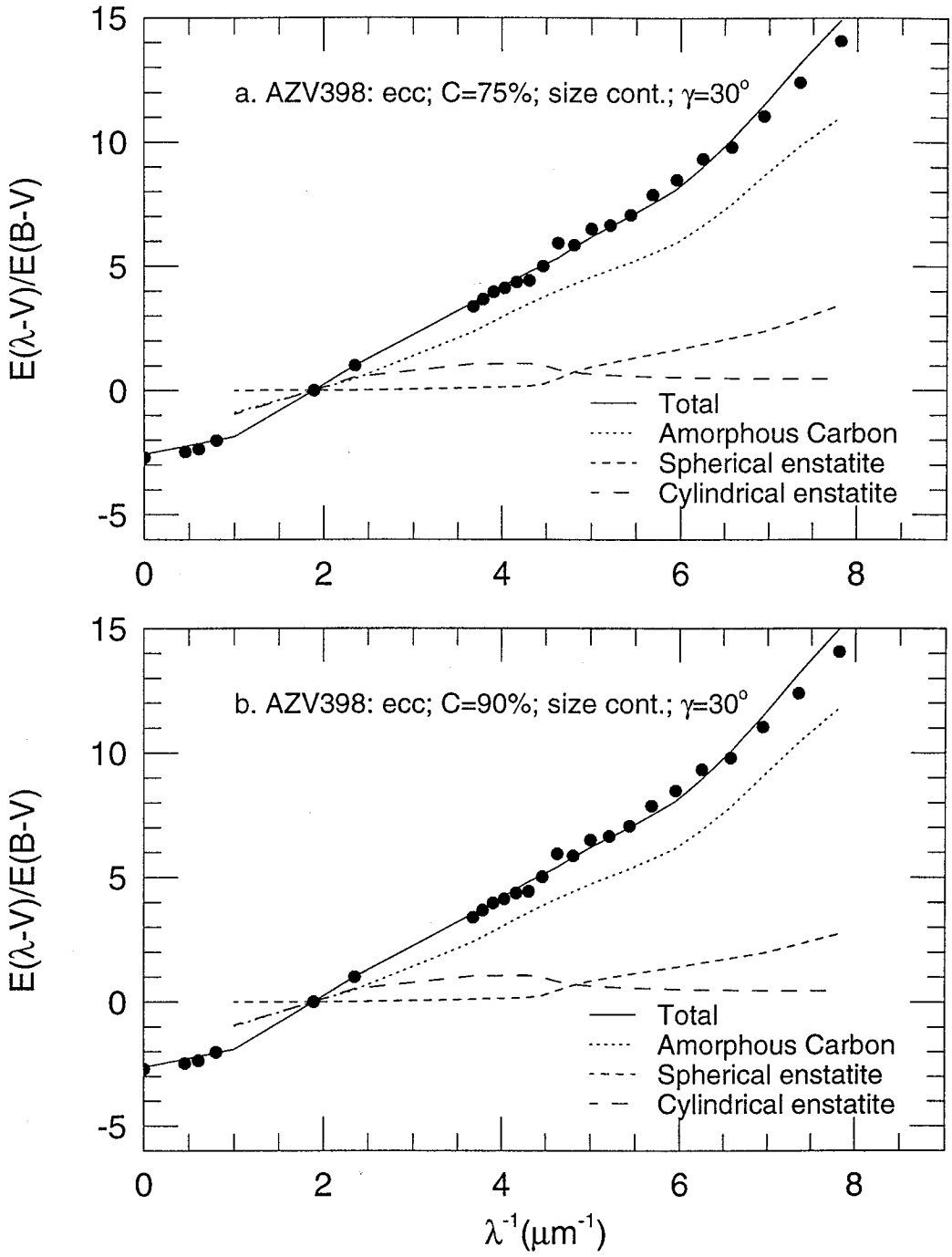

Fig. 19.— Two of the fits to the extinction data of AZV398 shown in Fig. 18. The contribution of each component to each of the extinction fits is shown. See caption to Fig. 18 and the text (sec. 3.3.1) for more details.

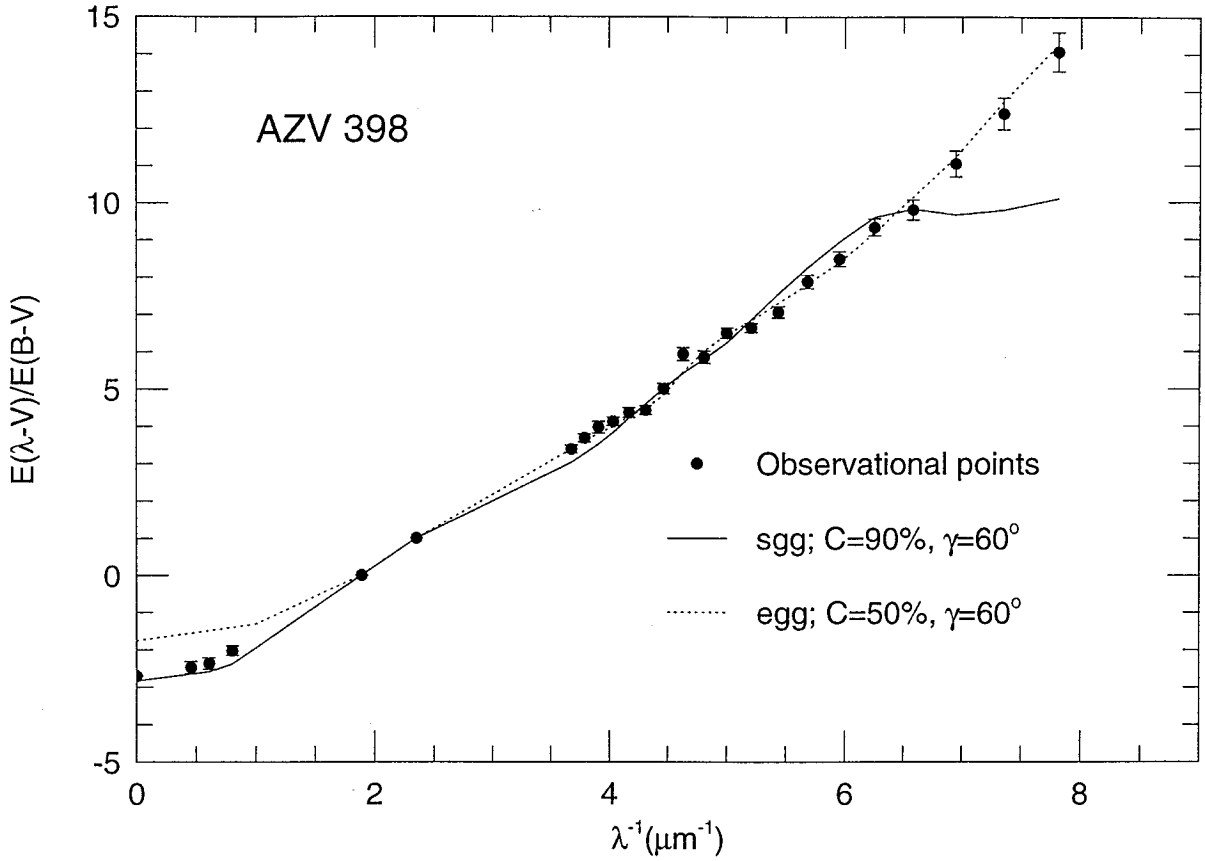

Fig. 20.— Fits to the extinction data of AZV398 using the CG model. Note the discrepancy in the FUV, when using astronomical silicate. Enstatite does not provide a good fit in the IR. The size distribution parameters used in the models are: $a_c = 0.0046\mu$m and $a_i = 0.060\mu$m for spherical silicates; $a_c = 0.024\mu$m and $a_i = 0.056\mu$m for cylindrical silicates; $a_c = 0.0053\mu$m and $a_i = 0.115\mu$m for graphite (**solid line**); $a_c = 0.00088\mu$m and $a_i = 0.038\mu$m for spherical silicates; $a_c = 0.051\mu$m and $a_i = 0.051\mu$m for cylindrical silicates; $a_c = 0.0035\mu$m and $a_i = 0.080\mu$m for graphite (**dotted line**).

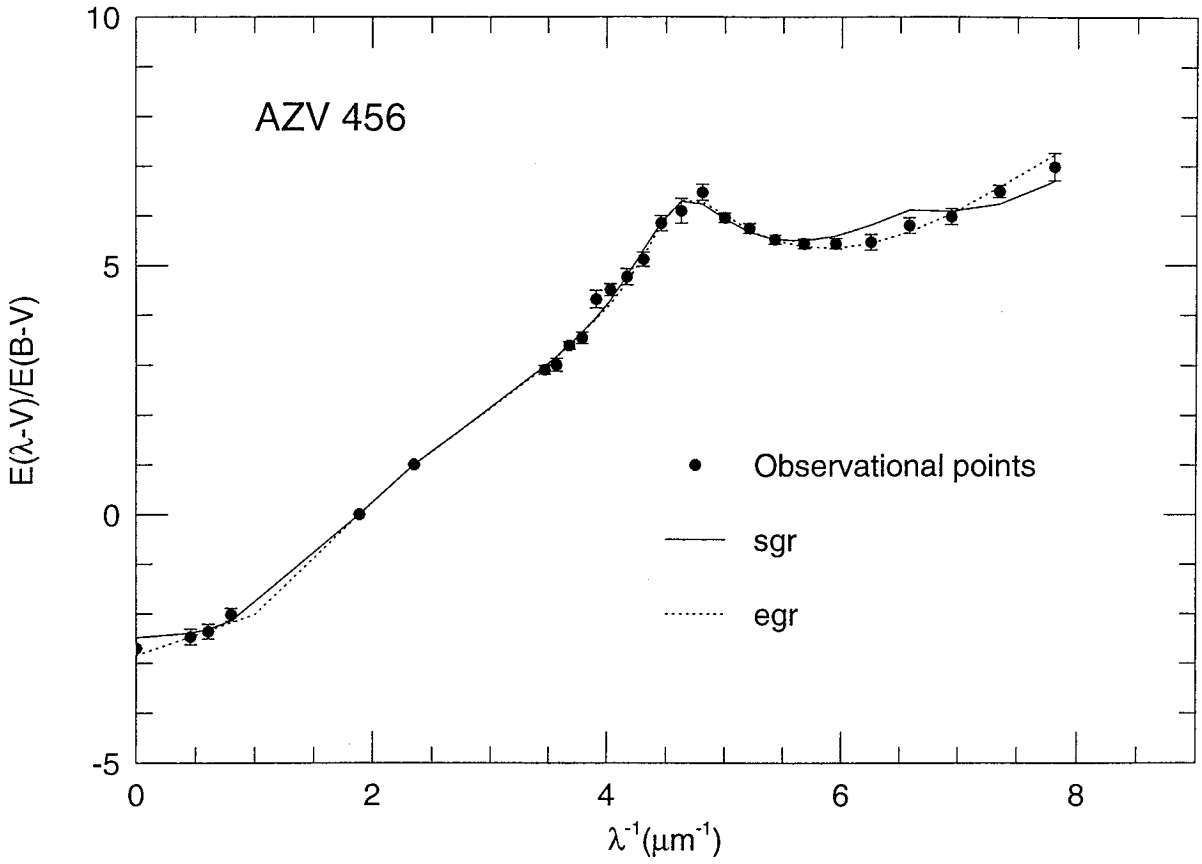

Fig. 21.— Fits to the extinction data of AZV456 using the MRN model with only spherical particles of graphite and silicate. In both curves, we have used 25% of carbon in grains. The size distribution parameters used in the models are: $a_-^{sil} = 0.018\mu$m, $a_p^{sil} = 0.26\mu$m, $a_-^{car} = 0.0018\mu$m and $a_+^{car} = 0.079\mu$m (**solid line**) and $a_-^{sil} = 0.015\mu$m, $a_p^{sil} = 0.29\mu$m, $a_-^{car} = 0.0039\mu$m and $a_+^{car} = 0.18\mu$m (**dotted line**).

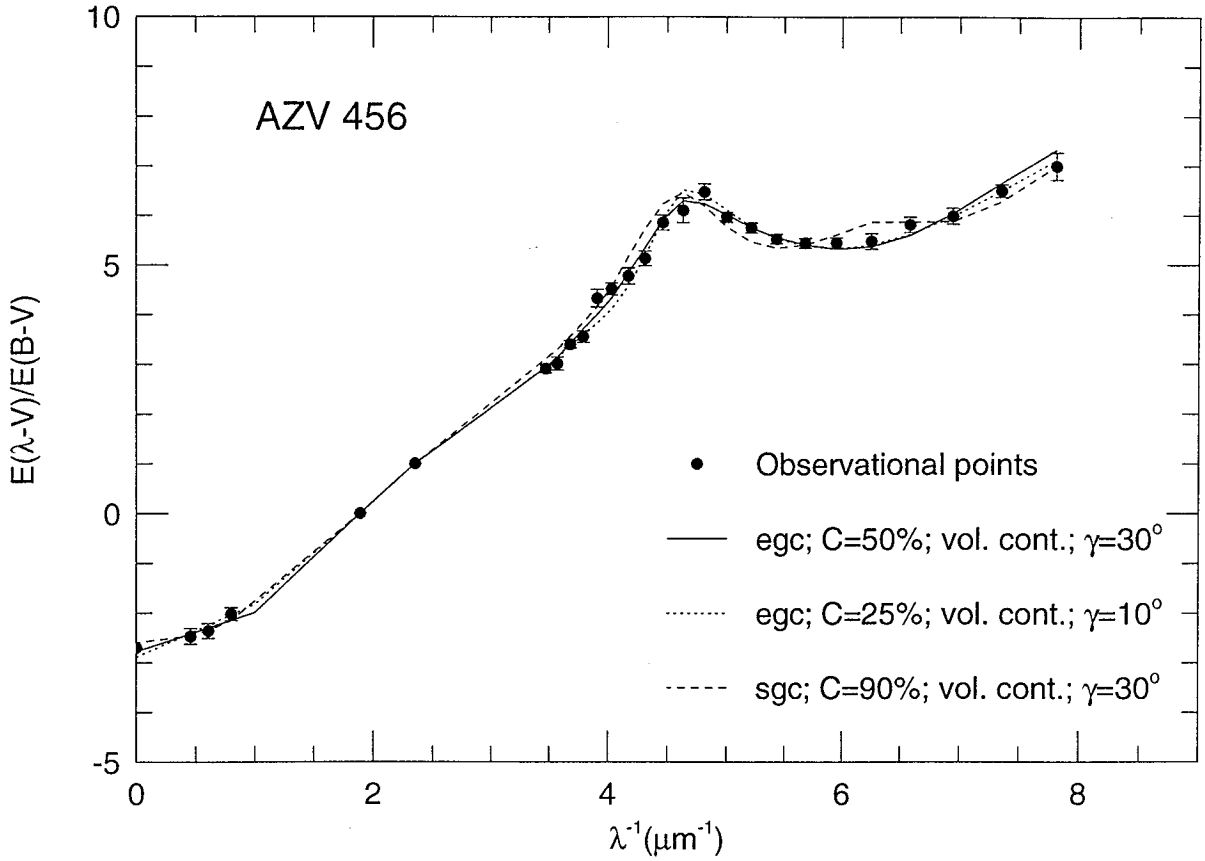

Fig. 22.— Fits to the extinction data of AZV456 using the MRN model with spherical graphite and silicate particles and cylindrical silicate particles of sizes adjusted by the polarization fits. The maximum size of the spherical silicate particles have been constrained by the distribution for cylindrical particles. In all curves, we have used volume continuity. Note the small differences in the region of the bump. The size distribution parameters used in the models are: $a_{-}^{sil} = 0.024\mu$m, $a_{p}^{sil} = 0.062\mu$m, $a_{+}^{sil} = 0.19\mu$m, $a_{-}^{car} = 0.018\mu$m and $a_{+}^{car} = 0.12\mu$m (**solid line**); $a_{-}^{sil} = 0.017\mu$m, $a_{p}^{sil} = 0.11\mu$m, $a_{+}^{sil} = 0.14\mu$m, $a_{-}^{car} = 0.0059\mu$m and $a_{+}^{car} = 0.15\mu$m (**dotted line**) and $a_{-}^{sil} = 0.027\mu$m, $a_{p}^{sil} = 0.056\mu$m, $a_{+}^{sil} = 0.16\mu$m, $a_{-}^{car} = 0.011\mu$m and $a_{+}^{car} = 0.11\mu$m (**dashed line**). See text (sec. 3.3.2) for more details.

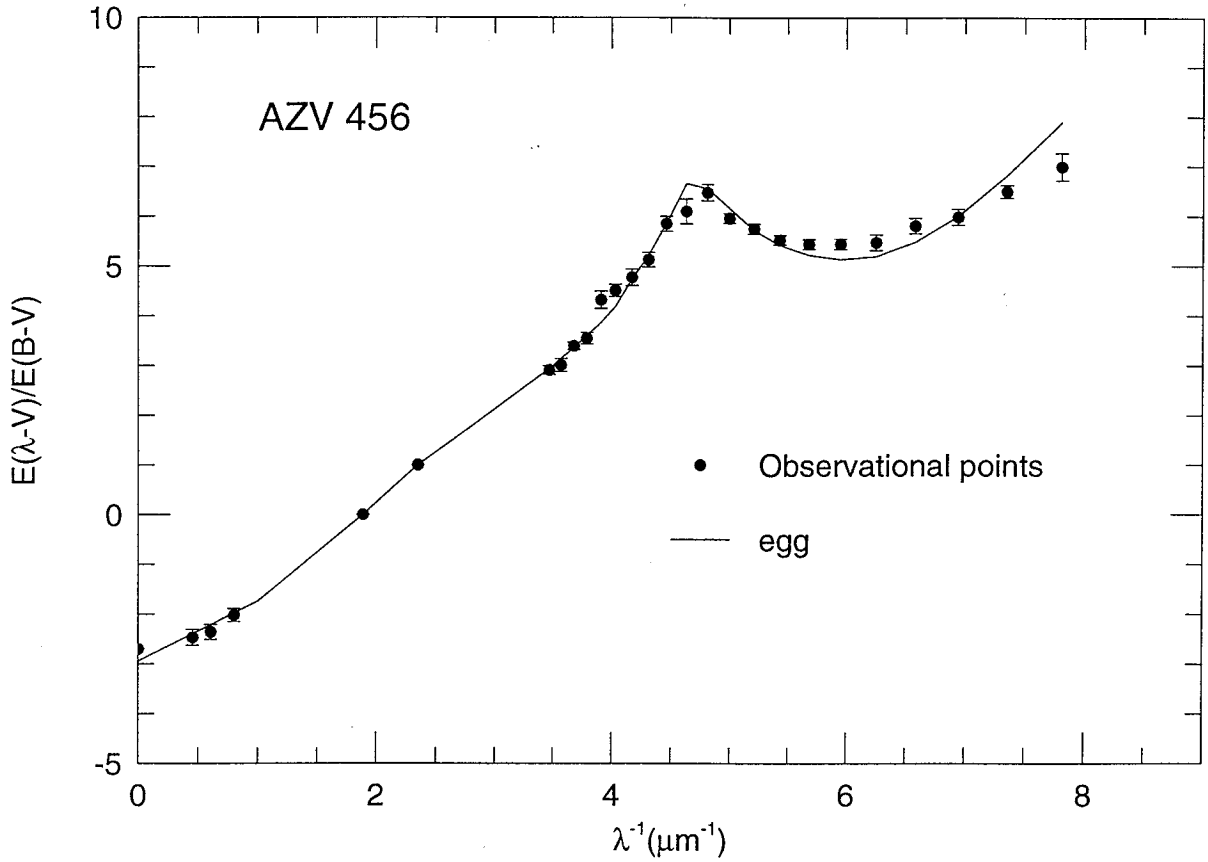

Fig. 23.— Best fit to the extinction data of AZV456 using the CG model. The size distribution parameters used in the models are: $a_c = 0.0047\mu$m and $a_i = 0.060\mu$m for spherical silicates; $a_c = 0.12\mu$m and $a_i = 0.028\mu$m for cylindrical silicates; $a_c = 0.0048\mu$m and $a_i = 0.049\mu$m for graphite (**solid line**).